In Situ ^{10}Be Ages from the Parallel Roads of Glen Roy – Loch Lomond Stadial Landforms

David Small

MSc Thesis

2008

Declaration

I, David Patrick Small, hereby declare that the work submitted in this thesis is my own except where referenced to the work of others.

Signed.....

Acknowledgements

I would like to thank my supervisor Dr Derek Fabel for formulating this masters project. I would also like to thank him for his patience and assistance throughout the year and for always being available when I needed help. I would also like to thank him for his assistance with some of the data figures in this thesis. The step by step guide to sample preparation is taken from the sample preparation handbook at SUERC. I would like to thank Maria Miguens-Rodriguez for her invaluable assistance in the laboratory as well as the AMS team at SUERC for analysing the samples and aiding with data reduction.

Contents

ABSTRACT 2

1. INTRODUCTION 3

2. *IN SITU PRODUCED* COSMOGENIC NUCLIDES AND THEIR APPLICATION 5

2.1 INTRODUCTION 5
2.2PRINCIPLES 6
2.2.1 Physics 6
2.2.2 Production Rates 9
2.3 CALCULATING PRODUCTION RATES 12
2.3.1 Scaling for altitude and latitude 12
2.3.2 Topographic shielding 13
2.3.3 Sample coverage 14
2.3.4 Sample thickness 14
2.4 ACCELERATOR MASS SPECTROMETRY (AMS) 15
2.5 CALCULATING EXPOSURE AGES 19
2.6 UNCERTAINTIES 20

3. THE PARALLEL ROADS OF GLEN ROY 23

3.1INTRODUCTION 23
3.2 RELATIONSHIP TO THE GLACIAL HISTORY OF SCOTLAND 23
3.3 SEQUENCE OF LAKE LEVEL CHANGES 26
3.4 SHORELINES AND ASSOCIATED FEATURES 27
3.5 TIME AVAILABLE FOR FORMATION 32
3.6 FINAL DRAINAGE OF THE LAKES 33
3.7 PALAEOSEISMICITY 35
3.8 AGE CONTROL 36

4. METHODOLOGY 38

4.1 SAMPLING STRATEGY 38
4.2 SAMPLING METHODOLOGY 40
4.3 SAMPLE PREPARATION 41
4.3.1 Quartz separation 42
4.3.2 Isotope extraction 42

5. RESULTS AND DISCUSSION 45

5.1 RESULTS 45
5.1.1 Interpretation of shoreline samples 48
5.1.2 Interpretation of fan samples 50
5.2 DISCUSSION 52
5.2.1 Rates of shoreline formation 52
5.2.2 Timing of LLS maximum ice extent 55
5.2.3 Timing of Fan and 260m shoreline Formation 57
5.2.4 Palaeoseismicity 59

6. CONCLUSION 60

7. APPENDICES 62

7.1 SAMPLE PREPARATION – STEP BY STEP 62
7.2 CHEMISTRY DATA 77
7.3 AMS DATA 78

Abstract

The Parallel Roads of Glen Roy along with their associated terraces and fans provide one of the best examples of the suite of features produced by the interactions of glacial, fluvial and lacustrine processes. These features have been the subject of numerous studies over many years and as a result are some of the best known geological features in the world. Despite this attention they have proven difficult to date using any of the absolute dating techniques available. Here we present the first absolute ages from the Parallel Roads using *in situ* ^{10}Be. We sampled from 9 different locations and 2 distinct geomorphologic settings, the 325m shoreline and 2 fans associated with the 260m shoreline. The ages obtained show good agreement within 1σ errors for each of the 2 settings. The shoreline ages indicate that each road was formed synchronously throughout the glen during the Loch Lomond Stadial (LLS). The ages from the fan samples indicate that deposition was occurring on these surfaces into the Holocene, which precludes the possibility that the fans are entirely pre-LLS features as has been previously argued. The ages obtained in this study also let us constrain the occurrence of a large (5.9) seismic event that occurred in this area around the time of shoreline formation to occurring before 11.3 ± 0.6 ka.

1. Introduction

Investigating a region's geomorphological history requires an understanding of features that can be attributed to certain processes or events. Such an understanding can allow a chronological history of landform and landscape development to be constructed provided there is some form of age control. This age control may be in the form of relative ages or may come from the use of absolute dating techniques to provide independent ages on certain landforms. Without numerical age control any attempt to construct a landscape history in terms of timing of events and process rates may be flawed and lead to inconsistencies within the larger geomorphologic setting.

The "Parallel Roads of Glen Roy" are world-renowned features located in the Central Highlands of Scotland. It has long been understood that they are the shorelines of former ice-dammed lakes (Jamieson 1863). Much work has been carried out in order to understand the processes and events that were associated with their formation. As a result we now have a good understanding of how the "roads" were formed as well as detailed measurements of their dimensions. Subsequently it has been possible to use this knowledge to investigate other geological problems such as the glacio-isostatic history of Scotland. The application of *apriori* knowledge to investigate glacio-isostasy is based on the conclusion that the "roads" are of Loch Lomond Stadial (LLS) age. This conclusion stems from the relationship between the roads and landforms related to Loch Lomond Stadial ice in Glen Roy.

However there is a complete lack of independent age control from the "roads" themselves. Attempts to date the roads using radiocarbon dating have proved unsuccessful due to a lack of suitable organic material. Palynological investigations have suggested a Late Glacial age but are inconclusive. Recent attempts to correlate the varve record of the

lake sediments to the GRIP Ice Core have proved more promising but only provide a floating chronology. As yet there are no published dates relating to the time of "road" formation.

The application of *in-situ* produced terrestrial cosmogenic nuclides (TCN's) provides an opportunity to rectify this by applying single nuclide exposure dating to the shorelines. To this end samples were collected from several locations and two distinct geomorphological situations in an attempt to obtain quantitative data to constrain the age of the "roads" independently. These independent ages verify the conclusion of a LLS age from previous work and help our understanding of the glacial evolution of Scotland around the time of "road" formation.

2. *In situ* produced terrestrial cosmogenic nuclides and their application

2.1 Introduction

According to Gosse & Phillips (2001) the first suggestion that incoming cosmic radiation could produce radioactive nuclides at the Earth's surface was made by Grosse (1934). Davis & Schaeffer (1955) developed this idea to propose that these in situ produced terrestrial cosmogenic nuclides could be utilised in the study of geological problems; specifically they speculated that measurement of 36Cl could be used to date Pleistocene glacial events. Initially the method was not developed further due primarily to the limitations of the available analytical techniques.

The development of Accelerator Mass Spectrometry (AMS) made it possible to make the precise measurements necessary to apply cosmogenic nuclides to geological questions. Over the past 20 years the technique has been developed for a variety of nuclides that are formed in situ in minerals exposed at the Earth's surface. These in situ produced terrestrial cosmogenic nuclides (TCN's) allow accurate dating of events over the past 10 Ma. Since the initial application for calculating surface exposure ages of Libyan desert glass using 10Be (Klein *et al* 1986) the surface exposure dating technique has been refined and applied to a wide range of geological materials using a variety of nuclides (^{10}Be, ^{36}Cl, ^{26}Al, ^{14}C, ^{21}Ne, ^{3}He) covering an age range of 10^2 to 10^7 years (Gosse & Phillips 2001 and references therein).

2.2 Principles

2.2.1 Physics

In situ terrestrial cosmogenic nuclides (TCN's) are produced by interactions of minerals with secondary cosmic radiation (Lal & Peters, 1967). This secondary radiation consists of particles formed by incoming galactic cosmic radiation (GCR). GCR is mainly made up of high energy nucleons (mostly protons), which produce nuclear disintegrations in the upper atmosphere resulting in a cosmic ray cascade (Fig. 2.1).

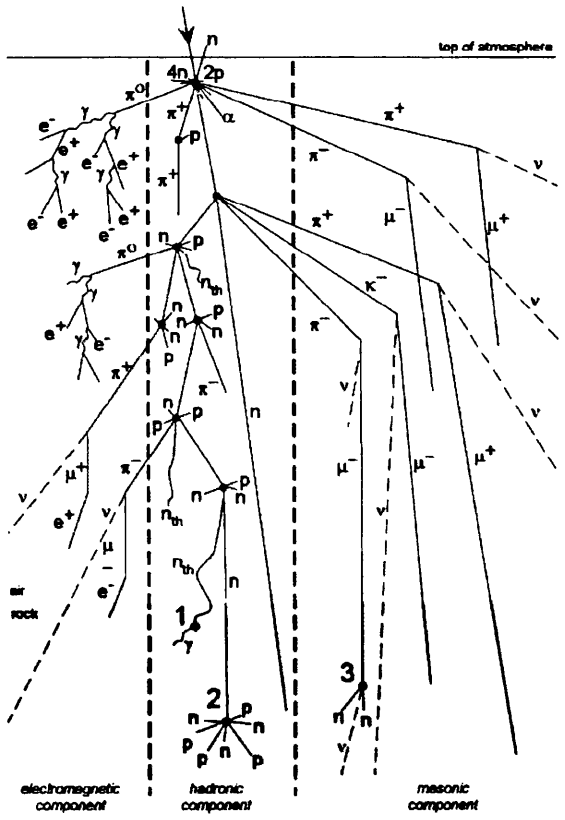

Figure 2.1. Diagram showing a cosmic ray cascade caused by a high energy nucleon entering the upper atmosphere. As can be seen only a small proportion of the radiation penetrates the Earth's surface. Numbers 1,2,3 refer to examples of in-situ cosmogenic nuclide interactions 1) $^{35}Cl \rightarrow ^{36}Cl$; 2) $^{16}O \rightarrow ^{10}Be$;3) $^{28}Si \rightarrow ^{27}Al$ (taken from Gosse & Philips, 2001).

Much of the secondary radiation is attenuated in the atmosphere but a significant proportion does reach the Earth's surface where it is composed mostly of neutrons and a smaller proportion of muons (Gosse & Phillips, 2001). It is these particles which produce

TCN's by several processes including; spallation, thermal neutron absorption and negative muon capture. Of these processes, spallation and muon capture are responsible for production of *in situ* ^{10}Be in quartz.

Spallation reactions are nuclear reactions occurring when high-energy nucleons, such as those neutrons formed in a cosmic ray cascade, collide with a target nucleus. The nuclei are excited to very high energies by this collision and nucleons or groups of nucleons escape until the residue is stable. This residual nuclide has a lower mass than the original target nucleus (Templeton, 1953). Within quartz, which is the mineral in which ^{10}Be is measured, the primary target nucleus for spallation reactions is ^{16}O although it can also be produced in Si (Nishiizumi *et al*, 1996). Muon capture occurs when a negative muon falls into the electron shell of an atom and is subsequently captured by the nucleus. The muon is captured by a proton within the atom leading to the production of a neutron thereby changing the atomic mass of the target nucleus resulting in the production of a cosmogenic isotope.

As a result of the different properties of the particles involved in spallation and muon capture, the relative importance of the processes changes with depth beneath the Earth's surface (Fig. 2.2). The high-energy nucleons involved in spallation are quite reactive and thus are mostly attenuated within the top few metres of the crust, in contrast the muons are weakly attenuated and therefore penetrate far deeper. The typical attenuation length of the high energy nucleons is 150-170 g cm^{-2} (Gosse & Phillips 2001). In comparison the attenuation length of muon production is 1500 g cm^{-2} (Gosse & Phillips 2001). This has the result that TCN production by muon capture becomes relatively more important as depth increases (Gosse & Phillips, 2001). At the surface it is estimated that muon capture accounts for only 1-3% of TCN production (Brown *et al*, 1995). These facts have the effect of limiting the production of TCN's to the top ~2m of the Earth's crust for ~20ka after a surface is initially exposed. If a surface has been stable for longer periods then muon capture will

have produced significant concentrations of TCN's at depths exceeding 2m due to the longer attenuation lengths associated with the particles responsible.

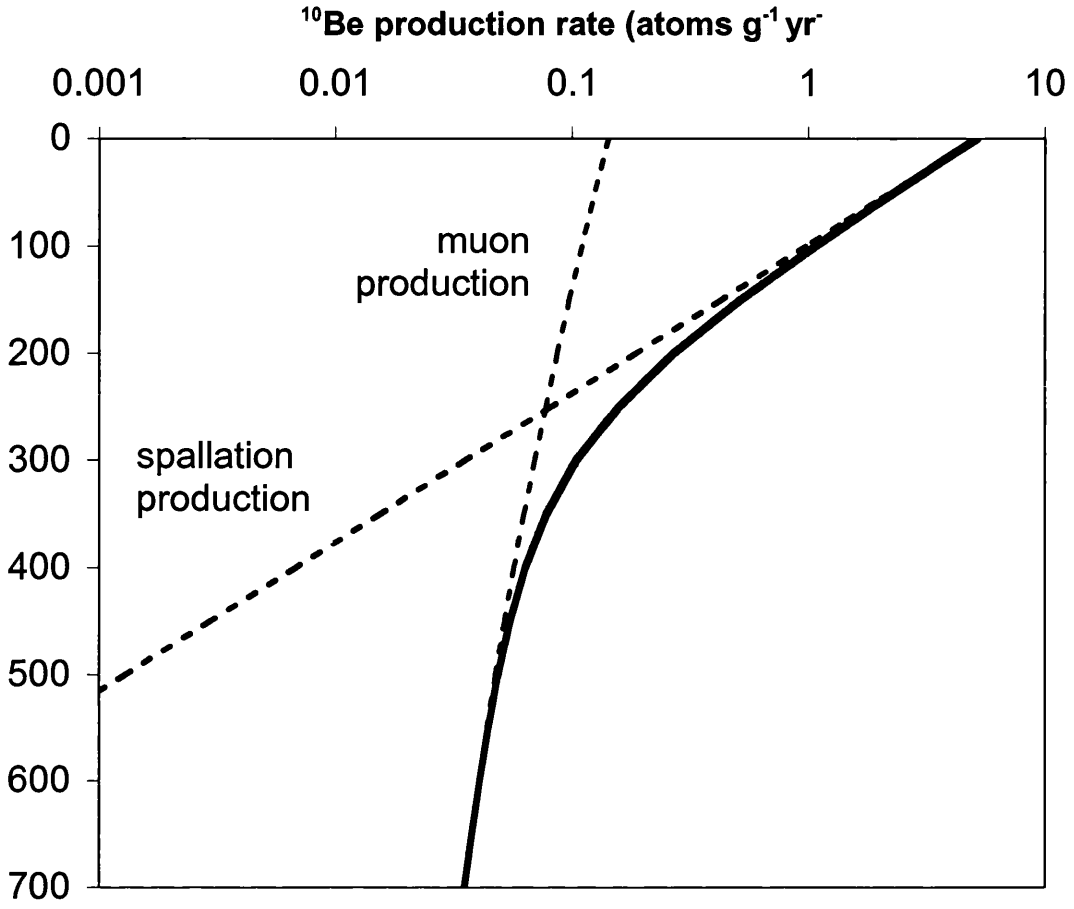

Figure 2.2. Diagram showing how the relative contributions of spallation and negative muon capture to the production rate of ^{10}Be change with depth within a quartz arenite at high latitude and sea level. It should be noted that the scale on the x-axis is exponential (after Gosse & Philips, 2001).

2.2.2 Production Rates

As a result of the reactions described in section 2.2.1, TCN's are produced in minerals exposed at or near the Earth's surface. In order to be able to apply knowledge of the TCN concentration of a sample it is essential to know the rate at which a particular TCN accumulates. This production rate depends on many factors including, and most importantly, latitude and altitude. This is due to the variance in the shielding effects of the geomagnetic field and the atmosphere respectively (Lal, 1991). As a result much work has gone into calculating TCN production rates and devising methods by which to scale them for specific geographic locations.

There have been several ways in which workers have attempted to establish TCN production rates. Firstly TCN concentrations have been measured in samples of a known exposure age, allowing calculation of an average production rate over the time of exposure (e.g. Nishiizumi *et al*, 1989). A second method used has been the calculation of production rates experimentally, for instance by exposing target materials of known composition to cosmic radiation for a controlled period of time (e.g. Nishiizumi *et al*, 1996). The third and final method adopted is to model production rates using complex theoretical models of particle production and transport (e.g. Masarik & Reedy, 1995)

Due to the dependence of production rates on latitude and altitude, any rates calculated from measurements are specific to the location where the samples were collected or the experiments were carried out. As a result it is necessary to standardise production rates and develop methods by which to scale these standardised rates for application in TCN studies in other locations. TCN production rates are standardised to sea level at high latitude (>50°) (SLHL). Rates are standardised to high latitude as here the effects of the Earth's magnetic field on TCN production are the smallest and thus it provides a useful reference frame for scaling other production rates. From this standard it is possible to calculate production rates

at a given latitude and altitude using published scaling factors (e.g. Lal 1991, Stone 2000, Dunai 2000).

Initial estimates of the production rates of ^{10}Be produced a value of 6.03 atoms g^{-1} yr^{-1} (atoms per gram of quartz per year) (SLHL) (Nishiizumi *et al*, 1989). This production rate was based on measurements of the nuclide concentration in glacially polished rocks in the Sierra Nevada, USA. Nishiizumi *et al* (1989) assigned an exposure age of 11000 cal yr. B.P to these surfaces based on published ^{14}C dates. Subsequent work by Clark *et al* (1995) and Clark & Gillespie (1997) demonstrated that the 11000 cal yr. B.P exposure age was too young by a couple of thousand years. Using a revised exposure age for the surfaces of 14000 cal yr B.P Clark *et al* (1995) calculated a production rate for ^{10}Be of 4.74 atoms g^{-1} yr^{-1} (SLHL). These lower production rates were supported by a measured ^{10}Be production rate of 4.76 ± 0.47 atoms g^{-1} yr^{-1} (SLHL) from a well dated terminal moraine in New Jersey (Clark *et al*, 1995).

Following this further high ^{10}Be production rates were reported by Nishiizumi *et al* (1996) [5.21 ± 0.29 atoms g^{-1} yr^{-1} (SLHL)] and Kubik *et al* (1998) [5.75 atoms g^{-1} yr^{-1} (SLHL)] which conflicted with the lower production rate reported by Clark *et al* (1995). Stone *et al* (1998) and Stone (1999, 2000) resolved this problem. They reported that the muonic component of production being used to calculate these production rates was too high. Lal (1991) assumed a muonic contribution to production of 15.6% based on the work of Nishiizumi *et al* (1989) and Lal (1988). The scaling factors he devised using this assumption are the ones that were used to calculate the high production rates mentioned previously. Stone (1999) corrected all the published rates for a revised muonic contribution of $3\% \pm 1\%$. Doing this he obtained a better agreement between published production rates. Stone (2000) gives a best-fit value for ^{10}Be production of 5.1 ± 0.3 atoms g^{-1} yr^{-1} (SLHL).

This value has recently been revised to 4.96 ± 0.45 atoms g^{-1} yr^{-1} (SLHL) (Balco *et al.* submitted).

A second problem with initial estimates of TCN production rates was that it was assumed that the Earth's geomagnetic field has remained constant over the periods of time to which TCN studies are applied. This is not the case (c.f. Masarik *et al* 2001) and corrections for geomagnetic field strength variations need to be made for studies in low latitudes where the effects of geomagnetic shielding are most sensitive to variations in field intensity. Such corrections do not need to be made to high latitude samples where the geomagnetic shielding has been effectively constant. This is because the magnetic field lines are mostly in the vertical direction and thus admits vertically incident radiation regardless of the intensity of the magnetic field (Desilets & Zreda 2003).

Several authors have addressed the issue of correcting production rates for variations in the intensity of the Earths magnetic field (e.g. Desilets & Zreda 2003, Pigati & Lifton 2004). It has been found that intensity corrected production rates for ^{10}Be can be ~30% higher for samples exposed over the past >25-30 Ka (Pigati & Lifton 2004). However intensity variations make little difference (<5%) on time integrated TCN production rates for samples with short (<~15ka) exposure ages (Pigati & Lifton 2004). Whether corrections should be made to account for temporal variations in the intensity of the Earth's magnetic field depends very much on the latitude of the sample site and the length of exposure being investigated.

2.3 Calculating Production Rates

2.3.1 Scaling for altitude and latitude

The published sea level and high latitude TCN production rates can be scaled for application in TCN studies at any location on the Earth's surface by using scaling factors for the latitude and altitude dependence of the cosmic ray flux. The most widely used scaling factors are those of Lal (1991). However in constructing these Lal made several assumptions which have prompted others to propose new scaling factors which address these mis-assumptions (e.g. Dunai 2000, Stone 2000).

Dunai (2000) derives a new set of scaling factors that take into account the effects of a non-dipole geomagnetic field. This differs from Lal (1991) who assumed that the Earth's magnetic field can be approximated as a dipole field. As cited by Dunai (2000), after 1958 it was accepted that a non-dipole field was necessary to accurately describe the cosmic ray flux at sea level. As a result of incorporating this in the calculation of his scaling factors Dunai produces factors which are up to 30% higher than those of Lal. The publication of these scaling factors prompted much debate (Desilets *et al* 2001, Dunai 2001), however the current calibration measurements are not accurate or extensive enough to support or refute either Dunai's or Lal's work (Stone 2000).

Another assumption of Lal (1991) is that the standard atmosphere model (c.f. Lide 1999) can be used to determine cosmic ray flux through the atmosphere (Gosse & Philips 2001). Stone (2000) points out that use of scaling factors based on this assumption in areas of persistent pressure anomalies will result in errors in exposure ages and production rates; in Antarctica these errors could be as large as 25-30% (Stone 2000). Stone re-calculated the scaling factors of Lal (1991) in terms of mean annual air pressure in order to be able to

correct for this. It is suggested that there should be a degree of consistency between the standardised production rate adopted and the scaling factors used. Given that we now know that there are several misassumptions used to calculate the scaling factors of Lal (1991) it is more desirable to adopt the most recently revised production rate of Balco *et al.* (submitted).

2.3.2 Topographic shielding

Once the production rate has been scaled to a particular sample location, it needs to be corrected for other factors that affect the cosmic ray flux to the sample. These are factors that act to shield the sample from the incoming cosmic radiation. Published TCN production rates assume production is occurring on a horizontal surface that is open to the entire sky. For this to be the case the inclination angle to the horizon has to be 0° for the full 360° rotation. Any surrounding topography that blocks part of the sky will serve to reduce the cosmic ray flux. Therefore once the production rates have been scaled for altitude and latitude they must be corrected for topographic shielding. This is done by calculation of a scaling factor that is the ratio of the actual radiation flux at the surface to the flux that would be present if the entire horizon were horizontal. Two methods for calculating this scaling factor have been proposed. Both involve making measurements of the angle of inclination to the horizon around the sample site (Dunne *et al* 1999; Gosse & Philips 2001). From these measurements it is possible to calculate the proportion of the sky blocked out by surrounding topography and calculate the radiation flux ratio. In general the effects of topographic shielding are relatively small, a sample at the bottom of an infinite cone with walls sloping at 45° would still receive 80% of the incoming radiation (Gosse & Philips 2001).

2.3.3 Sample coverage

In addition to topographic shielding a sample may be shielded from incoming cosmic radiation by overlying material such as snow, water, sediment etc. Correcting for such cover requires knowledge of the depth, duration and periodicity of the overlying material. As these are often not fully constrainable it may be necessary to make certain assumptions. For instance it may need to be assumed that a covering of peat formed instantaneously over a sample and that after formation its depth remained constant. The production rate P_x (atoms g^{-1} y^{-1}) at depth x (cm) can be expressed as an exponential function (Lal 1991):

$$P_x = P_0 \cdot e^{-(x\rho/\Lambda)} \qquad 1$$

where P_0 is the surface production rate, ρ is the density of the overlying material and Λ is the absorption mean free path (characteristically 150-170 g cm^{-2}; Gosse & Philips, 2001). This will give the nuclide production rate for the duration of coverage by overlying material. The duration may be constrained or it may need to be assumed depending on the availability of relevant data. If the coverage history is constrained it is possible to establish time dependent production rates and these can be used in conjunction with the measured TCN concentrations to correct apparent exposure ages (e.g. Stone *et al* 1996).

2.3.4 Sample thickness

Another feature of published production rates is that they are specified at the rock surface, thus even after corrections described in the previous section are carried out the revised production rate is specific to the uppermost surface of the sample. As mentioned in section *2.2.1* the particles involved in TCN production are attenuated with depth, thus the production profile varies with depth (Figure 2.2). As samples have a thickness it is necessary to integrate the surface production rate over the actual sample thickness using equation 1.

As we know the surface production rate after correction for altitude, latitude, topographic shielding and sample coverage we can assign P_0 a value of 1. This will have the effect of producing a correction factor for sample thickness. Therefore to correct for sample thickness we integrate:

$$\int_{x}^{0} e^{-(x\rho/\Lambda)} \qquad \mathbf{2}$$

Thus equation 2 becomes:

$$P_x = \frac{\Lambda}{\rho x} \cdot \left[1 - e^{(x\rho/\Lambda)}\right] \qquad \mathbf{3}$$

Solving equation 3 for sample thickness x (cm) will produce a correction factor by which to multiply the surface production rate P_0 (atoms g^{-1} y^{-1}). The resultant production rate is now specific to a particular sample as it has been corrected for altitude, latitude, topographic shielding, sample coverage and sample thickness. It is this production rate which is used with the measured TCN concentration to obtain an apparent exposure age.

2.4 Accelerator Mass Spectrometry (AMS)

It was not until the development of accelerator mass spectrometry (AMS) in the late 1970s (Nelson *et al.*, 1977; Bennett *et al.*, 1977) that the measurement of the very small quantities of cosmogenic isotopes could be realised as a routine technique. One of the most important features of AMS is the combination of the high efficiency of mass spectrometry technology, which can also discriminate against isobaric and molecular interferences, together with the ability to measure isotopic ratios for specific elements to a level of 1 in 10^{15}.

Fifield (1999) and Hotchkis et al. (2000) give excellent descriptions of the principles of operation of a tandem AMS system similar to the one used at SUERC, where the measurements for this study were made. The following summarises the operation and refers to parts of the AMS system shown in Figure 2.3. Negative ions are generated in the ion source (1) by sputtering the sample with caesium ions. The negative ions are then pre-accelerated to 30-200 keV, and mass analysed by the injection magnet (2). In the case of ^{14}C, ^{26}Al and ^{129}I, isobaric inferences are eliminated because ^{14}N, ^{26}Mg and ^{129}Xe do not form stable negative ions.

The negative ions are then accelerated to the positive high voltage terminal of the accelerator where they pass through a low pressure gas (e.g. argon). The purpose of this is to strip off electrons to convert the negative ions to multiple-charged positive ions and cause negative molecular ions to dissociate into their component atoms which also emerge positively charged. In the second stage of the tandem accelerator (3), the positively charged ions are accelerated back to ground potential. In the process they pass through the analysing magnet (4), which selects the ions of interest using a combination of charge state and energy and sends them to the detector. A fraction of the molecular fragments can also reach the detector as a result of charge changing collisions with gas molecules during the second acceleration stage. Most AMS systems therefore incorporate either a velocity filter or an electrostatic analyser to remove these.

The AMS determines the ratio of the rare isotope to an abundant isotope of the same element; $^{10}Be/^{9}Be$ for example. This is accomplished by accelerating ions of the abundant isotope or isotopes, as well as the rare isotope. Whereas the latter are counted individually, the former (which are typically 10^{12} times more intense) must be measured as an electrical current in a Faraday cup. The offset Faraday cup assembly (5) measures the abundant isotope (e.g. ^{9}Be), which is deflected more than the heavier, rare isotope (^{10}Be). The same principle

holds for carbon, aluminium, iodine, chlorine and other species. The rare isotopes are transported through a 20° electric cylindrical analyser (ECA) (6) and a ultra-thin SiN window to filter out any other possible interfering ions such as ^{10}B, an isobar of ^{10}Be, for an overall system sensitivity of better than 1 in 10^{15}. Interfering background levels are reduced to a few parts in 10^{16}. The rare isotope ions, which were selected through the analysing magnet and ECA, are counted in a gas ionisation detector (7). The gas is ionised by the collision with the high energy ions, and it is possible to analyse the target isotope ions separately by collecting and quantifying the electric charges. In this way ratios of $^{10}Be/^{9}Be$ are routinely measured with precisions of better than 4%.

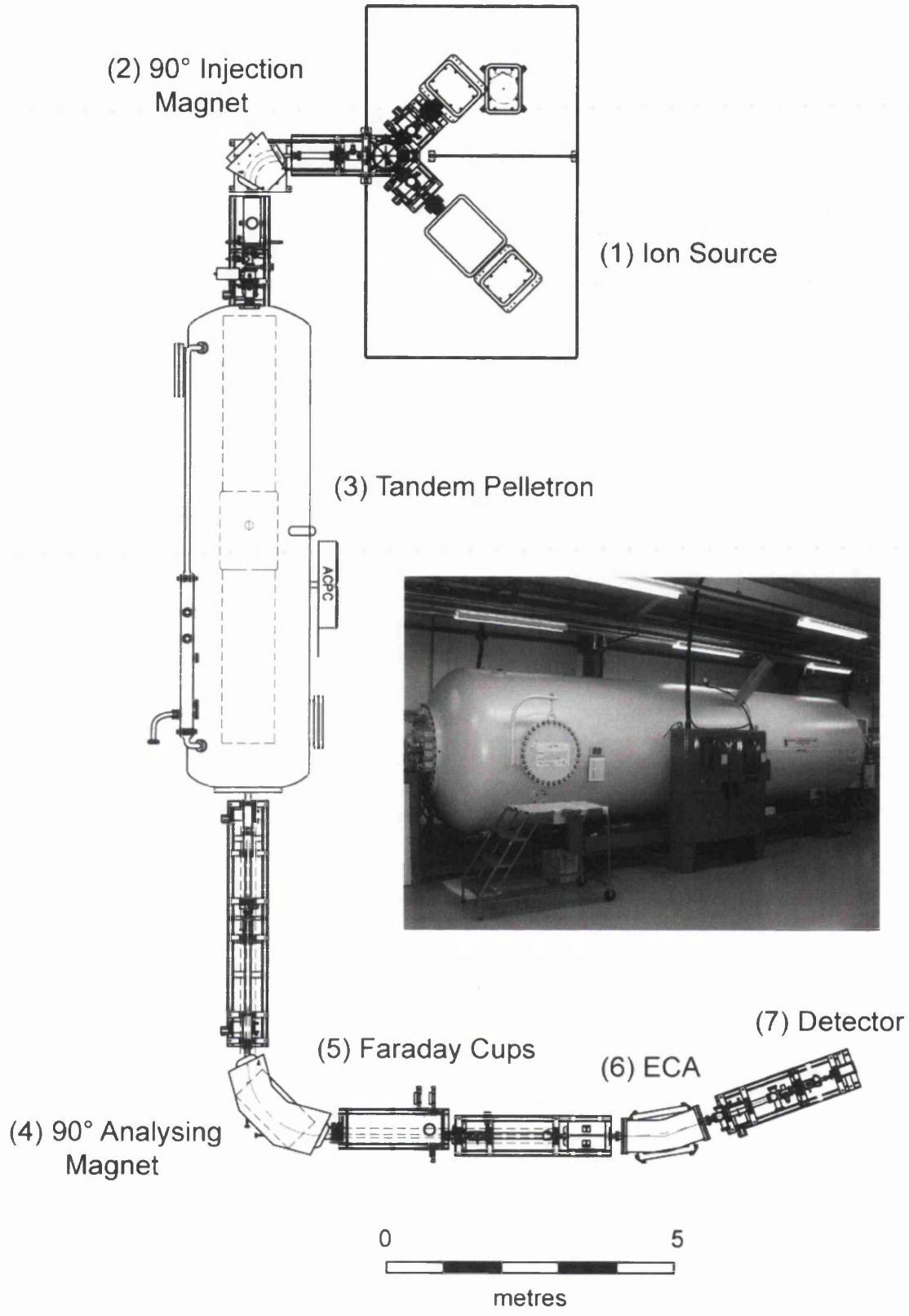

Figure 2.3 The 5MV NEC tandem pelletron accelerator at SUERC. The inset photo shows the 8.5 metre long accelerator pressure vessel.

2.5 Calculating exposure ages

In order to calculate exposure ages from the nuclide ratios as measured by AMS it is necessary to calculate the nuclide concentration N (atoms g^{-1}). This can be done using knowledge of the sample size and carrier spike added (see section 4.3.2) by applying the following equation:

$$N = \frac{\text{AMS Measurement } (x10^{-15}) \text{ x Be Carrier added } (\mu g) \text{ x } N_A}{\text{Sample mass(g) x } 9.0122} \quad \textbf{4}$$

Where the AMS measurement is in terms of the ^{10}Be:^{9}Be ratio and N_A is Avogadro's number (6.022×10^{23}). Addition of the Be carrier is discussed in Section 4.3.2. Knowing the nuclide concentration it is now possible to apply the sample specific production rate to calculate the apparent exposure age of a sample. This is done utilising the following equation derived from Lal (1991):

$$N = N_{inh}e^{-\lambda t} + \frac{P}{\lambda + \frac{\varepsilon\rho}{\Lambda}} \cdot \left(1 - e^{-\left(\lambda + \frac{\varepsilon\rho}{\Lambda}\right)t}\right) \quad \textbf{5}$$

where P is sample specific production rate (atoms g^{-1} y^{-1}), λ is the decay constant of the nuclide (yr^{-1}), t is time (y), ε is erosion rate (cm yr^{-1}) and N_{inh} is any cosmogenic nuclide concentration inherited from previous exposure. The other variables are the same as in equation 1. There are two unknown in this equation, time (t) and erosion rate (ε). We can only solve for one of these and have to make an assumption about the second. In the absence

of independent erosion rate measurements it is usual to assume the erosion rate is zero. Under this assumption equation 5 reduces to:

$$N = \frac{P}{\lambda} \cdot \left(1 - e^{-\lambda t}\right) + N_{inh} \qquad 6$$

In certain cases it is possible to assign N_{inh} a value of 0 as it can be assumed that the sample has had no prior exposure. This equation can be re-arranged to solve for t:

$$t = \left[\ln\left(1 - \frac{N\lambda}{P}\right) \right] / \lambda \qquad 7$$

This assumes that no erosion has occurred since the sample was exposed. This may be a reasonable assumption in certain geomorphic situations (e.g. striated, polished surfaces). Note that while striations indicate low post exposure erosion they do not tell us about how much material was removed prior to exposure so the surface may still have inheritance. In other situations post exposure erosion of the surface may have occurred and the apparent exposure age given by the above equation will underestimate the age of a sample surface as erosion physically removes cosmogenic nuclides and brings to the surface material that has been partially shielded during its period of exposure.

2.6 Uncertainties

When reporting ^{10}Be exposure ages two uncertainty values are often quoted; internal and external uncertainty. The larger value is the external uncertainty while the smaller value is the internal uncertainty.

The internal uncertainties, also known as the analytical uncertainties, are concerned with the measurements made in determining the nuclide concentration in the quartz sample. Thus, in theory, any measurement made during the sample processing and analyses could

contribute to the overall analytical uncertainty. In practise however only a limited number of sources make a significant contribution.

Fink *et al* (2006) derive the final analytical uncertainty in ^{10}Be concentrations from a quadrature sum of four sources of analytical uncertainty. These are; the standard mean error in the AMS measured $^{10}Be/^{9}Be$ ratio, the AMS reproducibility, the measurement of the ICP-AES Al quartz concentration during sample preparation (not relevant in studies where there is no Al analysis) and the uncertainty in the ^{9}Be carrier spike added. By combining these sources of uncertainty they obtain the value for the internal uncertainty. Balco (2006: available at http://hess.ess.washington.edu/math/docs/commo/ams_data_reduction.pdf) also presents a method to obtain the final analytical uncertainty. This method takes account of 3 sources of uncertainty; the uncertainty in the isotope ratio measured by AMS, uncertainty in the number of atoms in the procedural blanks and uncertainty in the carrier mass added.

The other source of uncertainty in exposure age calculations is systematic uncertainty. These are uncertainties in the theoretical knowledge that is applied in order to calculate exposure ages. There are two main sources of systematic uncertainty. Firstly the uncertainty in the reference production rates, and secondly, uncertainty in the scaling factors used for scaling these reference production rates to different latitudes and altitudes.

The external uncertainty reported with exposure ages takes into account both the systematic and analytical uncertainties. It is this value that must be considered when comparing exposure ages to calendar ages or dates derived from other techniques. Balco *et al* (submitted) also argue that the external uncertainty should be used when comparing ages from widely disparate locations as it is not known whether any one scaling scheme is more accurate for certain locations than an other.

The internal uncertainty only takes account of the analytical uncertainty. For comparison of ages within a study of limited spatial extent, such as the one presented here, only the

internal uncertainty needs to be considered for statistical comparisons. However, when comparing any surface exposure age with another dating technique, the external uncertainties should be quoted.

3. The Parallel Roads of Glen Roy

3.1 Introduction

The "Parallel Roads of Glen Roy" are some of the most famous geomorphological features in Scotland. Many historical figures visited Glen Roy and attempted to explain how these curious features had been formed (e.g. Darwin 1839). It was the classic paper of Jamieson (1863), and his subsequent additional comments of 1892, which first elucidated the sequence of events in Glen Roy and its vicinity that led to the formation of the parallel roads. This work was later expanded upon by others (e.g. Sissons 1978,1979a,b; Sissons & Cornish 1982) to provide a detailed explanation of the sequence of events that led to the formation of the parallel roads as well as the way in which the roads themselves were formed. Other more recent work has focussed on attempts to date the roads (Lowe & Cairns 1991) and how they can be used to investigate palaeoseismicity and glacio-isostatic rebound (e.g. Ringrose 1989, Dawson *et al* 2002).

3.2 Relationship to the Glacial History of Scotland

The term "parallel roads" is used to refer to a suite of features in Glens Roy, Gloy and Spean. All of these features are associated with the existence of former ice-dammed lakes in this area. Thus an understanding of how these lakes came into being is essential in order to be able to place the parallel roads into a broader geomorphological and glacial historical context.

The parallel roads are generally accepted to have formed during the Loch Lomond Stadial (LLS) which is approximately equivalent to the Younger Dryas (YD) of Scandinavia (12.7-

11.5 cal ka B.P). During this period ice accumulated in the Western Scottish highlands and occupied the Great Glen from South of Loch Ness (Sissons 1981). Figure 3.1 shows the maximum ice extent in Scotland during the LLS (Hubbard 1999). Glacial erratics and striae show that ice sourced from the west crossed the Great Glen in the Spean Bridge area (Peacock 1970). This ice mass, often referred to as the Spean Glacier (Figure 3.2), flowed in an easterly direction to occupy large parts of Glen Spean and, at its maximum extent, the lower parts of Glen Roy (Peacock 1970, Sissons 1979a). The ice occupying Glen Gloy was derived from the glacier occupying the Great Glen.

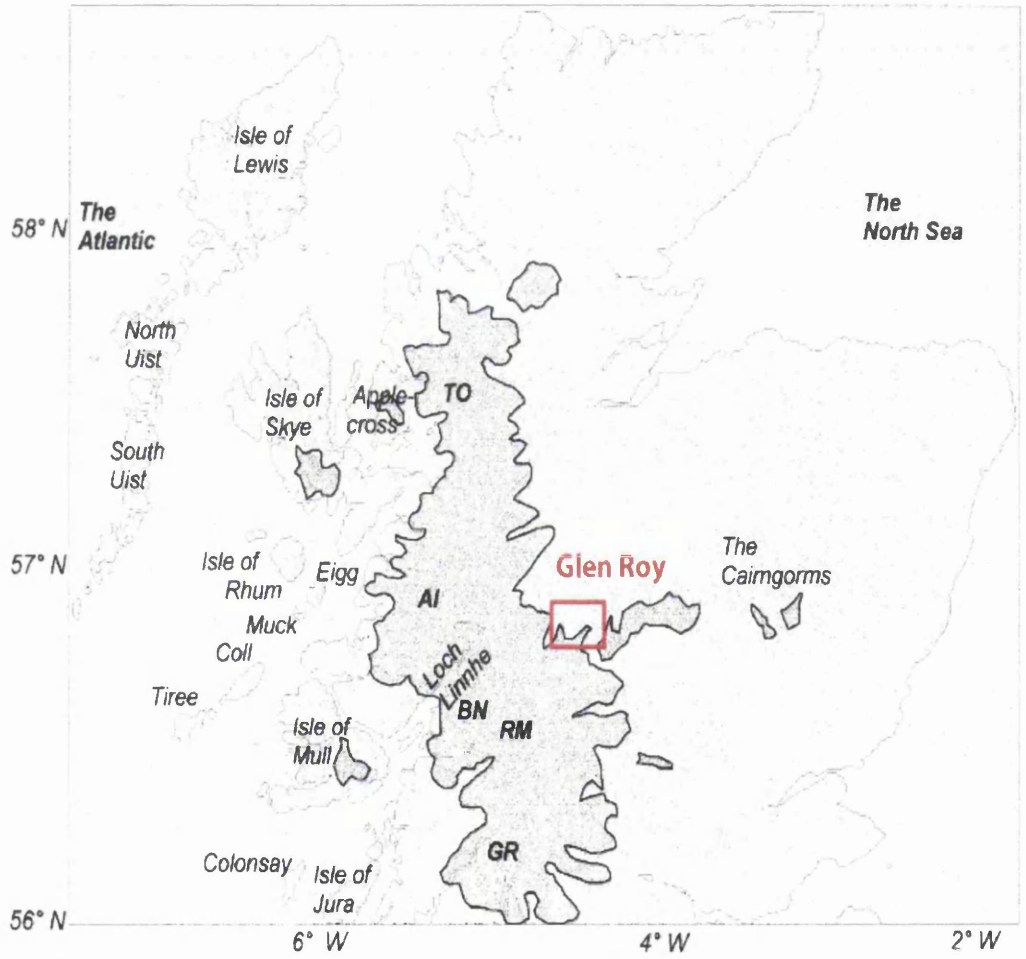

Figure 3.1. Map showing the maximum extent of ice in Scotland during the Loch Lomond Stadial with the Glen Roy area highlighted. The letters refer to the work published on ice extent in individual areas. Torridon (TO), Ailort (AI), Ben Nevis (BN), Rannoch Moor (RM), Southwest Grampians (GR). Taken from Hubbard (1999).

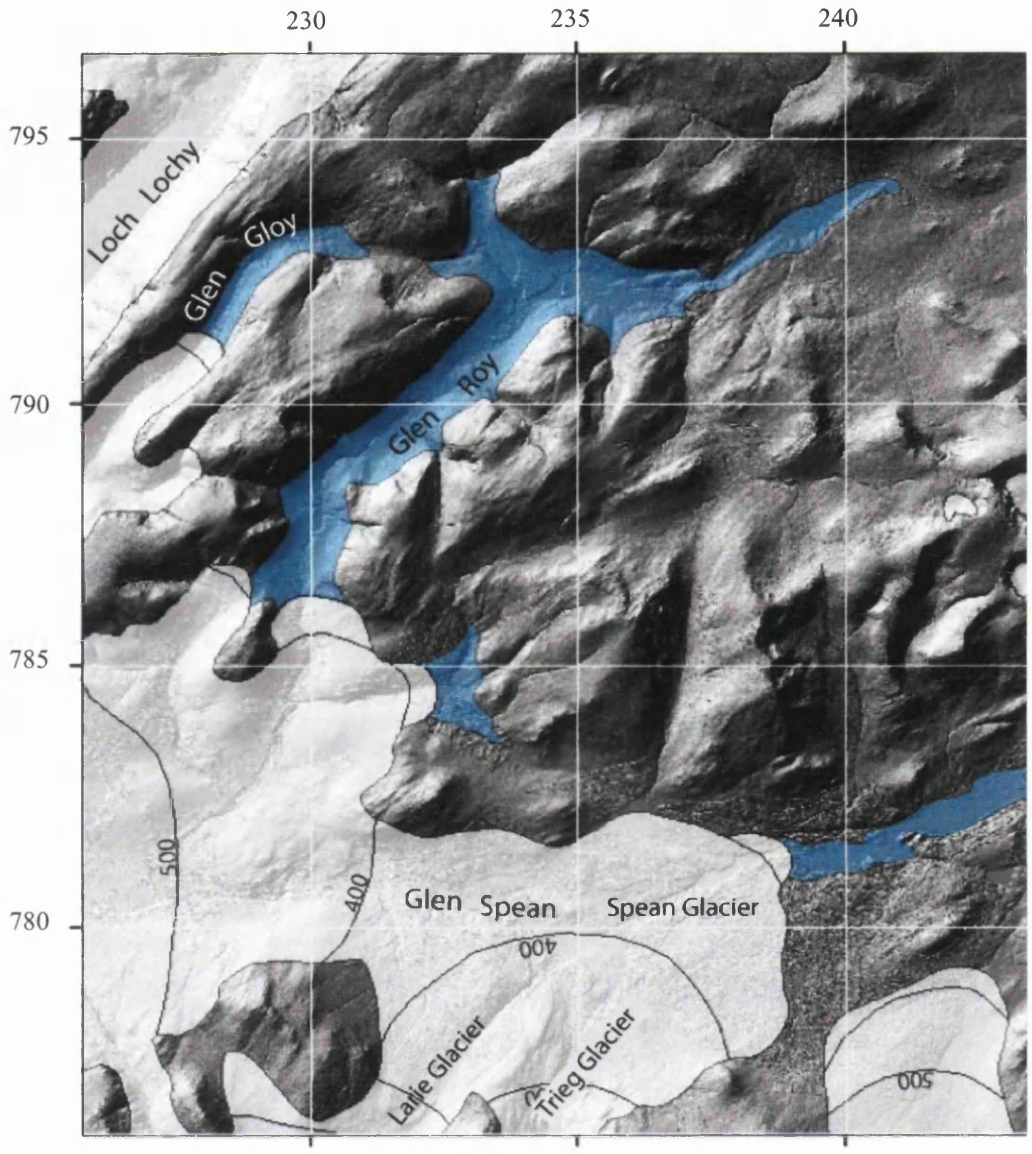

Figure 3.2. Map showing the maximum ice extent in the Glen Roy area. Diagram courtesy of A.G Finlayson, adapted from Sisson (1979a). The base map is copyright BGS/NERC (data provided by Intermap Technologies, 2003).

The ice located in Glen Spean coalesced with ice that was nourished to the south of the Ben Nevis Range (Sissons 1979a). The two most important glaciers were the Laire Glacier and the Trieg Glacier (Figure 3.2). The north facing corries of the Ben Nevis Range did not make a large contribution to the Spean Glacier. Only in the west of the range did ice from corries join the main Spean ice mass (Sissons 1979a). Some of the corries in the east of the range failed to nourish glaciers despite being of similar altitude. This SW-NE contrast is

also seen to the east of Glen Roy where Sissons (1979a) records evidence for only a few corrie glaciers. Of these only the one in Coire Ardair was thought to have exceeded 0.5km in length. Recent work has suggested ice in this area was more extensive (Finlayson 2006) however the SW-NE contrast is still well developed.

These contrasts in glacier distribution point to an increasing ELA from SW-NE across Scotland during the LLS. Sissons (1980) reconstructed ELA's in the Western Highlands. The ELA's to the south and southwest are as low as 300m whereas to the northeast they rise to over 800m. Sissons (1979a) concludes that these vast differences within a small area reflect variations in the distribution of snowfall during the LLS. These variations are due to the weather patterns prevalent at this time (cf. Sissons 1980). To the southwest snowfall was far greater, this meant that glaciers nourished in these areas were of far greater volume and intruded north and north-easterly into areas of much lesser snowfall. It is the intrusion of such glaciers into Glens Roy, Gloy and Spean that dammed the drainage system and formed the ice-dammed lakes to which the roads are related.

3.3 Sequence of Lake Level Changes

As the Spean glacier advanced into Glen Spean it blocked drainage to the southwest and led to the establishment of an ice-dammed lake at 260m in Glens Spean and Roy. The level of this lake was controlled by the height of its overflow at its eastern end. This overflow was at the present the eastern end of Loch Laggan. Loch Laggan presently drains westwards but at the time of the ice dammed lakes the drainage was reversed. As ice advanced into lower Glen Roy it cut off this overflow and the lake level in Glen Roy rose to 325m. Overflow from this lake was now via the 325m col between Creag Dubh and Beinn Teallach, into a much-reduced lake at 260m that still existed in Loch Laggan area. Further advancement of

ice into Glen Roy subsequently cut off the col at 325m and the lake level in Glen Roy rose further to 350m while a small lake at 325m still existed in the side valley of Gleann Glas Dhoire. The 350m lake level was controlled by the height of the col at the head of Glen Roy, the overflow via this col drained northeast into the Spey Valley (Figure 3.3).

This series of lake level changes is referred to as 'the rising sequence' (Sissons 1978). As ice retreated from Glens Roy and Spean at the end of the LLS the series of lake level changes was reversed and this is referred to as the 'falling sequence' (Sissons 1978). The lake level in Glen Gloy was constant at 355m as the col between Glen Gloy and Glen Roy is the lowest in the drainage system, similarly the lake level in Glen Spean was constant at 260m during the time of the rising and falling sequences in Glen Roy.

The three principal roads in Glen Roy are at 260m, 325m and 350m (Figure 3.3). These roads all correspond to the height of the cols that controlled the lake levels. Although other faint roads do exist they do not correspond to the height of cols (Sissons 1981). Thus while the lakes must have existed at other levels it is likely that only the levels associated with the cols would have existed for any significant length of time and it is these lake levels with which the clearly formed roads are associated.

3.4 Shorelines and associated features

The parallel roads are predominantly the shorelines of the former ice dammed lakes, although in some places they are palaeo fluvial and palaeo fluvio-glacial features (Gordon 1993). Sissons (1978) carried out a detailed study of the three principal roads in Glen Roy. By analysing the nature of the material that makes up the roads he concluded that the roads were principally formed by erosion at the back and deposition at the front. Lateral transport

of fluvially derived material is not significant as the effects of river supplied material diminish away from streams within a few hundred metres (Sissons 1978).

In many places the shorelines are cut into bedrock, good examples of bedrock cut shorelines can be seen at Braigh Bac (GR306882), Creagan na Gaoithe (GR370925) and north of the Burn of Agie (GR369921). Jamieson (1863) invoked wave action as the mechanism by which the backslopes of the shoreline were eroded. However, Sissons (1978) argues against wave action being the only process acting to form the shorelines. He points out that the narrowness of Glen Roy would mean that the available fetch for many sections of shoreline would have been very short. In addition to this the glen sides are very steep and Sissons (1978) argues that it would be difficult to envisage the initiation of shoreline development on such steep slopes by waves generated over such short fetches. Sissons (1978) also points to the lack of basal notches and other features that might be formed by wave action as evidence that the process is not the sole agent of formation.

Instead Sissons (1978) concludes that frost action would have been an important factor in the formation of the shorelines. The climate at the time of the shoreline formation would have been severe and periglacial weathering processes would have occurred on a large scale. Sissons (1978) points to a site (GR370925) where the 325m shoreline continues around a rocky knoll and is continually backed by a cliff 1-5 metres high. Around this knoll the available fetch would have varied greatly, yet the shoreline is well formed in all alignments. It would be difficult to attribute this consistency in shoreline development to wave action because the variance in available fetches would likely have resulted in vastly differing wave sizes.

However Sissons (1978) did record a correlation between road volume (Figure 3.4) and those sections of shoreline exposed to a south-westerly fetch.

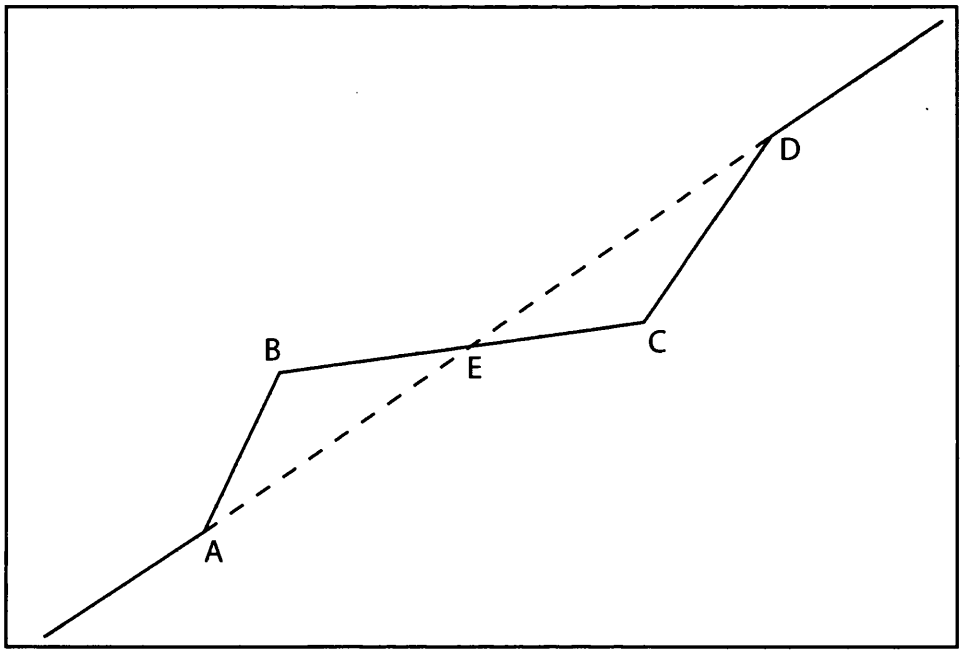

Figure 3.4 Schematic diagram explaining road volume. The volume of a shoreline (road) at any given point is calculated by making measurements (slope angle & distance) which allow the areas of triangles ABE and ECD to be calculated. The road volume is the sum of these areas, in effect the volume of material eroded from the backslope of the shoreline combined with the volume of material deposited on the foreslope. (Sissons 1978)

While it may initially seem that this correlation would support the view that wave action was predominantly responsible for shoreline formation Sissons (1978) argues that it can be explained in terms of frost action being the dominant process. He argues that the debris created by powerful frost action would be incorporated into ice forming on the lake surface. When this ice broke up, strong winds being funnelled along the glen would be effective in moving the loose ice and thus removing the material derived from frost shattering. Due to this process, sections of shoreline exposed to a south-westerly fetch could be envisaged to have had more material removed and thus have larger volumes. It is the combination of this process and, to a lesser extent, wave action that results in the strong statistical correlation between road volume and south-westerly fetch (Sissons 1978).

There has been little subsequent work on the processes involved in the formation of the shorelines although frost action has been argued to be an important process for the initiation of bedrock cut shorelines in other glacially dammed lakes (Dawson *et al* 1987). Therefore it

seems reasonable that the processes proposed by Sissons (1978) could account for the formation of bedrock cut shorelines in Glen Roy and vicinity.

In localised situations the parallel roads are not lake shorelines but result from fluvial and fluvio-glacial deposition. For example, west of the River Trieg in Glen Spean the 260m road is a kame terrace (Sissons 1978). In Glen Roy itself deltas occur where rivers carrying abundant gravel grade material entered the ice dammed lakes. Such features are generally only related to the 260m lake level as those deposited in the higher lake levels have been largely destroyed by fluvial erosion and land sliding (Sissons & Cornish 1983). Of these features three fans in upper Glen Roy are particularly impressive. These are known as the Turret Fan, the Brunachan Fan (Figure 3.5) and the Reinich Fan.

Figure 3.5. Photograph of the Brunachan Fan. The three pricncipal "roads" can be seen on the hillside to the upper right of the fan. Photograph from www.scottishgeology.com

Sissons & Cornish (1983) conclude that these fans were mostly deposited in the 260m lake of the rising sequence due to the presence of overlying laminated silts and clays which are interpreted as being the lake floor deposits of the 325m and 350m lakes. By the time the lake returned to the 260m level, at the end of the falling sequence, the volumes of gravel

being deposited by the rivers were much less due to a decrease in torrential input associated with spring melt (Sissons & Cornish 1983). These later gravels only extend over the uppermost portions of the fans and are not mantled by lake sediments (Sissons & Cornish 1983). In addition to their interpretation of the fans as being mostly sub-aqueous in origin Sissons & Cornish (1983) argue that the largest of the three fans, the Turret Fan, is a glacio-fluvial outwash deposit. They associate this deposit with the Gloy glacier, which at its maximal extent is thought to have crossed the Roy-Gloy col at the time of the 260m lake of the rising sequence.

Peacock (1986) rejects these interpretations. He interprets the fans as predating the parallel roads and of being subaerial in origin. These conclusions are based on sedimentological evidence. Peacock (1986) argues that the sedimentary structures indicative of sub-aqueous deposition (e.g. interbedded laminated silts and clays, turbidites etc.) are absent from the fan deposits and thus the fans were deposited subaerially prior to the existence of the lakes. Peacock (1986) concludes that the Turret Fan was deposited at a late stage of the retreat of ice from the Late Devensian maximum rather than during the LLS. The Brunachan and Reinich fans were interpreted as having been deposited during the period between deglaciation and the LLS. However he does not provide an explanation for the fans surfaces being coincident with the height of the lowest parallel road. This fact would appear to indicate that the fans were graded to a base level at 260m and it could be argued that only if the 260m lake was in existence would this be the case.

Subsequent pollen-stratigraphical studies have indicated an absence of late-glacial sediments at several key sites. These sites have yielded pollen sequences that are characteristic of the LLS/Flandrian transition at the Gloy-Roy col (Lowe & Cairns 1991). This evidence is used to support the interpretation of Sissons & Cornish (1983) that the Turret Fan was deposited during the LLS. If it was deposited prior to this time then it may

have been expected that earlier sediments would have been deposited at the col. However, it may be the case that the effect of water draining over this col at the time of the lake existing in Glen Gloy scoured away any earlier sediments. Thus it is not possible to definitively reject or accept either hypothesis without some independent age control regarding the time the fans were deposited.

3.5 Time available for formation

It is intuitive to realise that certain sections of a given road did not have the same length of time available to form as other sections. Near the ice margin that was in existence when a lake fell from a given level the road had much less time to form than elsewhere (Sissons 1978). For example, in Lower Glen Roy the 325m road exists between the final positions of the ice dams that held up the 350m and 325m lakes. This means that this section of the road must have formed during the falling sequence as the ice retreated from the location of the final 350m dam to the position of the final 325m dam. It also means that it had far less time to form than the sections of the 325m dam in upper Glen Roy where the 325m lake was in existence for much longer. This situation is repeated for section's of the 260m road that exist between the final positions of the 325m and 260m ice dams. It thus might be expected that the roads would fade as you approach the position of the former ice margin. However Sissons (1978) reports that this is not always so. He noted several examples where a road maintains its average width to within a very short distance of the ice margin.

In addition to differences in time available for formation of sections of the same road there must also have been differences between the time available for formation of the different individual roads. Sissons (1978) points out that the 325m road was formed while the ice advanced and retreated by about 1.5km while the 260m roads comparable figure is

8km. Despite the varying time that was available for road formation (both between sections of an individual road and between roads of differing heights) there is no great differences in the dimensions because each road was formed quickly and thereafter developed very slowly (Sissons 1978).

Evidence for the periods of time available comes from detailed examination of the varve record in the lake floor sediments deposited while the ice dammed lakes were in existence. Detailed analysis of the varve characteristics has allowed inferences to be made on how long the lake existed at each individual level. This work suggests that the 350m and 325m lakes were in existence for 137 years and 203 years respectively, while the 260m lake was in existence for 185 years (Palmer pers. comm.). While not resolving how long any individual section of road had to form, this data does concur with the conclusions of Sissons (1978) that the roads were formed quickly.

3.6 Final drainage of the lakes

The 350m and 325m lake levels of the falling sequence drained when the ice dam holding them up retreated beyond the cols of the respective heights. Thus, while drainage of these lakes was probably catastrophic it would have primarily been achieved with little or no subglacial component. Drainage of the final 260m lake however has been interpreted as being catastrophic and entirely by subglacial routes, a classic jökulhlaup (Sissons 1979b, 1981). The routes by which this lake drained and the deposits associated with it have been the subject of several published papers (e.g. Sissons 1979b, Russell & Marren 1998).

The final location of the ice margin damming the 260m lake is placed approximately at the location of the termination of the 260m parallel road on the northern and southern sides of Glen Spean (Sissons 1979b). Sissons calculates that the lake associated with this ice dam

would have been 35km long, with a volume of ~5km^3. Initial drainage of this lake is inferred to have occurred via the Spean gorge which starts approximately 2km west of Spean Bridge and runs NNW towards Gairlochy, from here the water followed the course of the Great Glen north-east towards Inverness (Sissons 1979b). Deposits along the inferred route of this jökulhlaup have been studied by Sissons (1979a,b) and Russell & Marren (1998). Initial work by Sissons (1979a,b) interpreted these deposits as jökulhlaup deposits based on general morphology and position. More detailed sedimentological work by Russell & Marren (1998) showed conclusively that the deposits were consistent with deposition by jökulhlaup. That this event occurred after LLS ice had retreated from its maximum extent is shown by the fact that the jökulhlaup deposits occur within the LLS ice limit as mapped by Sissons (1979a) and Bennet & Boulton (1993).

Following initial drainage of the 260m lake it is postulated that there existed a series of lakes at levels below 260m (Sissons 1979b, Russell & Marren 1998). These have been inferred to have drained via the Lundy Channel which runs west from ~6km south of Spean Bridge by periodic jökulhlaup (Russell & Marren 1998). This route for meltwater has a higher entrance than the Spean Gorge and thus for the entirety of its operation the ice dammed lake would have been unable to drain completely (Sissons 1979b). The change in drainage to the Lundy Channel is believed to be associated with the change in geometry and flow direction of the Spean Glacier on its retreat from the position of the 260m ice-dam. This led to a hydraulic gradient favouring drainage west via the Lundy Channel rather than north-west via the Spean Gorge (Russell *et al* 2003).

Following abandonment of the Lundy Channel a lake existed at 113m in Lower Glen Spean, shown by the relationship of the Spean river terraces (Sissons 1979b). This is the final lake in this area and it is believed to have overflowed north until the final collapse of the ice-dam and associated jökulhlaup (Sissons 1979b).

3.7 Palaeoseismicity

Although the roads are referred to by their height as if this is consistent across their length there does exist a degree of variability. Sissons & Cornish (1982) report that the height of the top (350m) road varies between 349.5m and 351.9m, the middle road (325m) varies between 324.5m and 326.8m, and the bottom road (260m) varies between 260.1m and 262.4m. They record that the largest deviation from the 'normal' altitude of each shoreline is associated with a fault on the north-west side of upper Glen Roy. They conclude that this displacement is the result of movement of the fault related to glacio-isostatic uplift. Due to the undeformed nature of the river terrace deposited by the River Roy immediately following final drainage of the 260m lake it is concluded that the pronounced differential uplift in the area had ceased by this time (Sissons & Cornish 1982).

Displacement of the roads was also observed by Dawson *et al* (2003), who report regional patterns of vertical shoreline displacement associated with glacio-isostatic tilting. In addition to this they record that some of the shoreline fragments have been affected by tectonic activity. Ringrose (1989a) also reported evidence for seismic activity in the form of deformation structure in the lake sediments deposited on the floor of the ice-dammed lakes. He interpreted two separate tectonic events from sedimentological evidence, the latter of which occurred near the end of lake sedimentation. Using an equation relating earthquake magnitude to the distribution of liquefaction, Ringrose (1989a) calculates that the minimum magnitude required to account for the observed pattern in the Glen Roy area is 5.9 (Richter scale).

It is considered likely by both Ringrose (1989a) and Dawson *et al* (2002) that the tectonic activity responsible for the shoreline displacement is related to glacio-isostatic rebound,

however the possibility that at least one of the episodes of tectonism is related to lake drainage cannot be ruled out (Peacock & Cornish 1989).

3.8 Age Control

Despite the large amount of work that has been carried out on the 'parallel roads' there remains a lack of independent age control on their time of formation. The age of the roads has been inferred using indirect evidence of the time at which the lakes, to which the shorelines are related, were in existence and the relationship between the roads and features interpreted as being of LLS age.

Palynological evidence (Lowe & Cairns 1991) from several sites only records sediments characteristic of the LLS-Flandrian transition. Nowhere do they record any older sediments. This suggests that the lakes were in existence during the LLS. If they were not it may be expected that sediments pre-dating the LLS would be recorded from sites lying within the inferred lake limits as sedimentation would have been possible if no lake was present during this time. However Lowe & Cairns (1991) point out that several of their sites are situated on the cols which acted as spillways for the lakes and any sediments pre-dating the LLS could have been removed by the scouring action of the overflow from the lakes. While this evidence demonstrates the likelihood that the lakes existed during the LLS it does not preclude the possibility that lakes existed in this area at a time prior to this.

Glaciological evidence (e.g. Sissons 1979b, Peacock & Cornish 1989) shows that in places the lateral extent of the roads corresponds to the position of features associated with ice margins. For example the lateral limit of the 325m road in lower Glen Roy is closely associated with a major cross valley moraine that is interpreted as recording the response of the ice dam as the lake level dropped from 325m to 260m (Peacock & Cornish 1989). That

the mapped features in Glen Roy are LLS in age is inferred from the mapped LLS ice limits dated by ^{14}C near Loch Lomond (Sissons 1979a). However there are no ^{14}C dates published for any glacial features in Glen Roy and vicinity and attempts to date the deposits of the roads themselves and associated fans have proved unsuccessful (Sissons 1979a, Ringrose 1989).

Recently work has been carried out on the varves present in the lake floor deposits of the ice-dammed lake. Assessment of these varves allowed a correlation of the Glen Roy varve record to the GRIP ice core (Palmer *et al* 2007). This correlation indicates that the Glen Roy varves were deposited during Greenland Stadial 1 (GS-1) which is roughly equivalent to the LLS in Scotland. However the varve chronology is a floating chronology as there are no independent constraints on when lake sedimentation began or ceased.

Taken together these lines of evidence suggest that the roads are LLS in age. However they do not prove conclusively that the roads are not partially inherited features dating from the latter stages of retreat from the Last Glacial Maximum. It is conceivable that during this retreat the distribution of ice was such that it allowed lakes to form at one or more of the levels associated with the parallel roads. If this occurred then it may have led to the formation of a shoreline at this level(s). While it may be expected that within the LLS ice limits any pre-existing shoreline(s) would be destroyed by glacial erosion, outside these limits such a shoreline may have survived more or less intact to be re-occupied by the lakes during the LLS. As it is thought the roads were formed quickly and thereafter developed slowly (Sissons 1978) it is possible that this re-occupation did not significantly alter the morphology of any pre-existing shoreline. As a result it would be morphologically similar to the younger shorelines. Therefore without independent age controls on the individual shorelines it is not possible to say conclusively whether they all date from the LLS.

4. Methodology

4.1 Sampling strategy

In this study the aim is to date the formation of former lake shorelines and to date the deposition of fluvial/fluvio-glacial fans which are associated with the lowest of the former lake shorelines. To do this bedrock samples with potential exposure ages thought to reflect the time of shoreline formation were collected from the shorelines. The attenuation of cosmic rays with depth effectively limits the production of TCN's in young (<20ka) samples to the top ~2m of the Earths crust (Section 2.2.1). If shoreline formation has resulted in removal of >2m of rock then the apparent exposure age of the sample can be expected to reflect the age of the shoreline. Removal of this amount of material can be inferred by measuring the angle from the downhill break of slope of the shoreline to the top of the backing cliff and then applying simple trigonometry to calculate the depth of exhumation due to shoreline formation (Figure 4.1).

Boulder samples were taken from the surfaces of the fans (Figure 4.2) on the basis that their apparent exposure ages would give a minimum age for the formation of the fans assuming that the boulders had not been emplaced on the fan surface at a later date by some other process. Samples were collected at sufficient distance from surrounding hillslopes to minimise the possibility that the materials had been deposited by gravity flows.

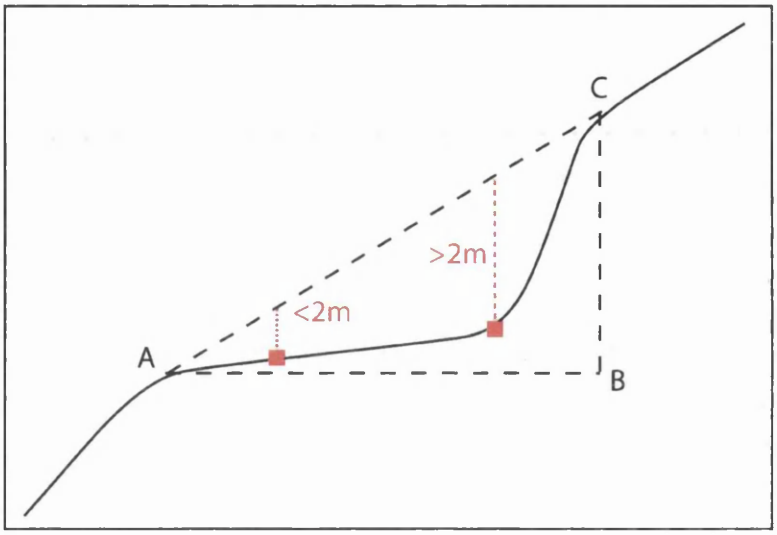

Figure 4.1. The height of the backing cliff on a section of shoreline was assessed by measuring angle CAB and distance AB. Simple trigonometry can then be applied to calculate distance BC. The squares indicate possible sample locations.

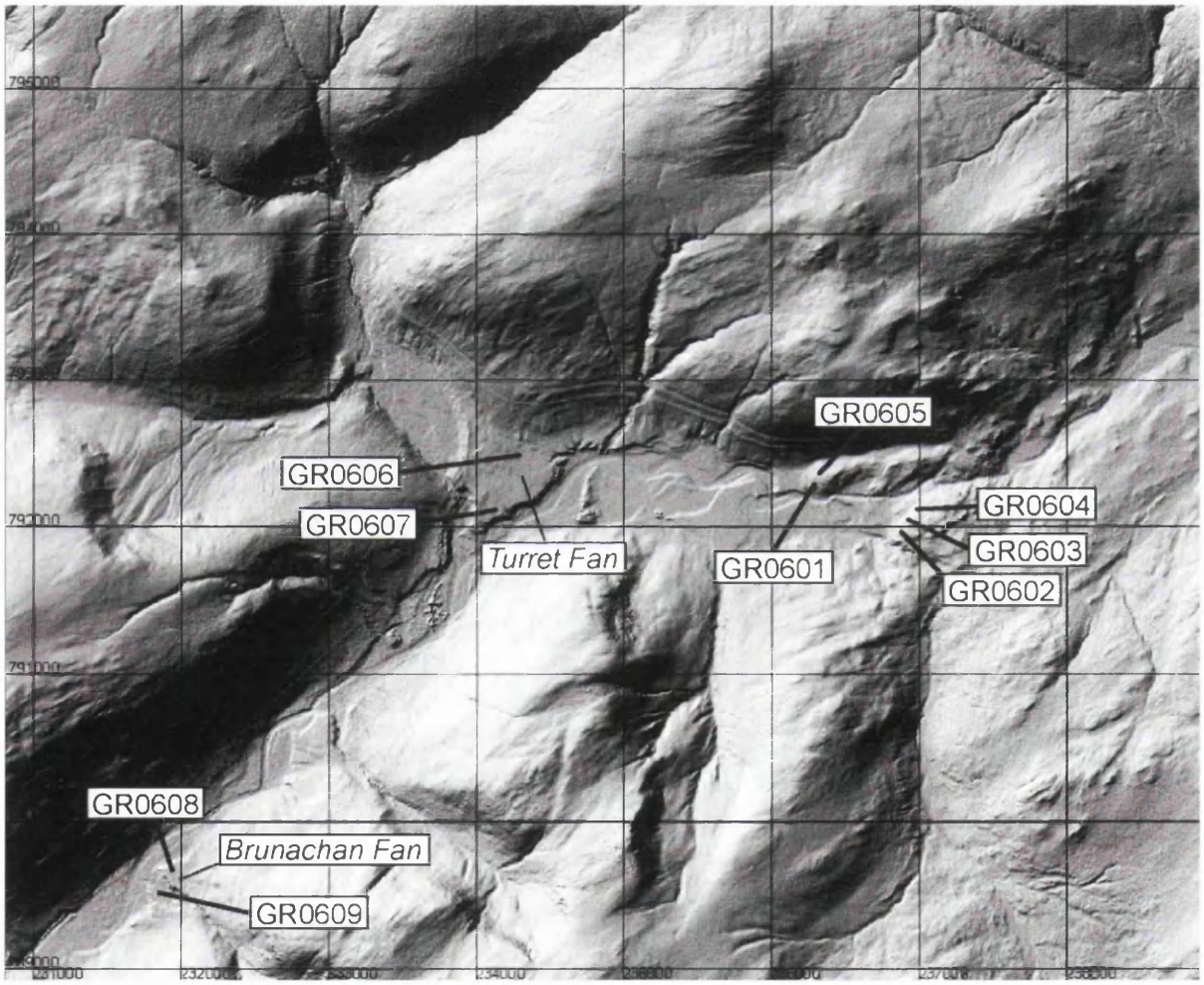

Figure 4.2 Digital elevation model of upper Glen Roy near the confluence with Glen Turret showing the location of the samples taken in this study. The base map is copyright BGS/NERC (data provided by Intermap Technologies, 2003).

It is necessary to assume that the samples were not exposed prior to deposition on the fan surface. If this were the case they could yield an apparent exposure age that pre-dates fan formation as the total TCN concentration would result from both this exposure and the exposure since deposition on the fan surface. The accuracy of an exposure age from such a sample must be assessed in context with the exposure ages of other samples in order to determine whether its apparent exposure age can be interpreted as reflecting the time of fan formation.

4.2 Sampling methodology

The shoreline samples were collected from the base of the backing cliff using a hammer and chisel. In one case it was necessary to dig down through a covering layer of peat to reach the bedrock (GR0605 and Table 5.1). The fan samples were collected in the form of whole clasts, except in one case where the sample was collected from the top surface of a boulder present on the fan surface. The sample locations were recorded using a hand-held GPS and the altitudes taken from topographic maps (Figure 4.2).

The shielding geometry of the sample was measured by dividing the skyline into sections defined by breaks in slope and measuring the angle of inclination and azimuth to each major break in slope (Figure 4.3). This data was recorded to allow calculation of a geometric shielding correction factor following the procedure of Dunne *et al* (1999). This uses the measurements of azimuth and inclination to calculate the proportion of the sky blocked by surrounding topography and hence the proportion of incoming cosmic radiation that is being prevented from reaching the sample. When a sample was taken from the base of the backing cliff the shielding geometry was more complex to measure. The backing cliff acts to block out a significant proportion of the sky. In effect it acts like a near infinitely high wall as only

vertically incident radiation or radiation from the lee direction can reach the sample location. Following sample collection in the field the samples were returned to the laboratory for processing.

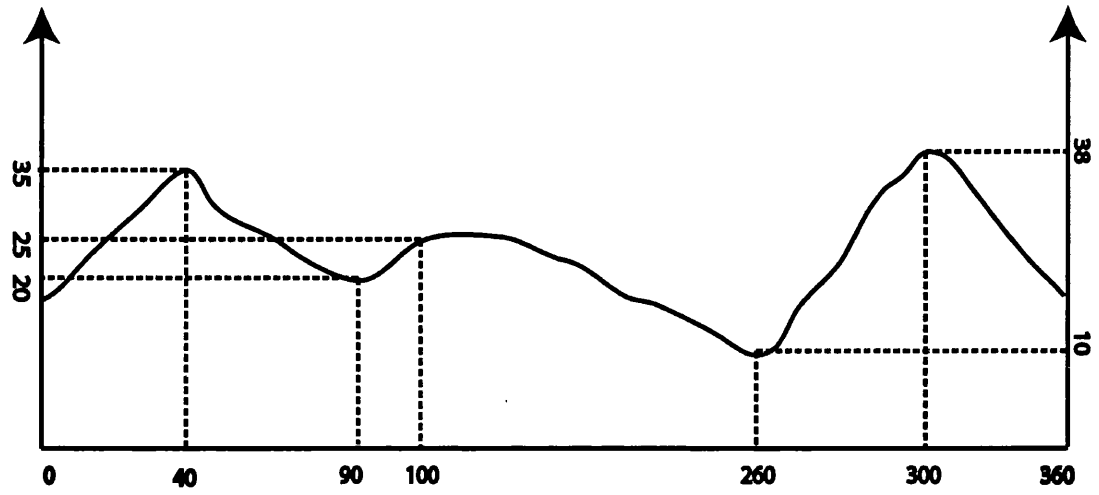

Figure 4.3. Sketch showing how to measure skyline inclinations in order to calculate geometric shielding. The black line is an idealised 360°panorama. The various dashed lines show the measurements of azimuth and inclination to each major break in slope. The horizontal and vertical axes are not to scale.

4.3 Sample Preparation

Once the samples are collected they need to be prepared for AMS analysis. The aims of this preparation are to transform the sample material into a form suitable for analysis and to concentrate the nuclide of interest so that it can be accurately analysed (Gosse & Philips 2001). The procedures followed in this study are those developed by Kohl & Nishiizumi (1992) and modified by Dr Derek Fabel at the Glasgow University - Scottish Universities Environmental Research Centre (GU-SUERC) cosmogenic icotope laboratories. These differ in some of the steps from other published procedures (e.g. Bierman *et al* 2003) but makes use of the same chemical principles. The procedure consists of 2 distinct phases; quartz separation and purification followed by isotope extraction and isolation. Figure 4.4 is a schematic depiction of the stages involved in sample preparation. Samples for ^{10}Be and ^{26}Al analysis are processed together due to the fact that the chemistry required to extract

them is similar. However this study focuses on Be and Al will not be discussed further. What follows is a brief overview of the cleaning and chemical separation stages involved. For a batch of 9 samples, as is the case in this study, the whole process of quartz separation, cleaning and isotope extraction takes around 4 months for a trained person.

4.3.1 Quartz separation

The individual samples are crushed until the grains are predominantly monominerallic. The 250-500μm fraction is then rinsed to remove fines and organics. Once dry the sample then undergoes magnetic and heavy liquid separation to concentrate quartz with respect to other minerals. Following this the samples are etched in dilute Hydrofluoric Acid (HF) which dissolves alumino-silicate minerals that would not be separated from quartz using physical methods. The leaching also etches the surfaces of the quartz grains removing meteoric ^{10}Be on the grain surfaces. After several HF leaches the samples are assessed for quartz purity by determining the Al content of the cleaned quartz using atomic absorption spectrometry. A low Al content (10-100ppm) is desirable since higher Al concentrations often indicate the presence of feldspars. Once the quartz is of acceptable purity the samples are ready to move onto the second phase of sample preparation where Be is extracted from the quartz and prepared for AMS analysis.

4.3.2 Isotope extraction

Since Be is a very rare element in quartz it is necessary to spike the pure quartz samples with a known amount of ^{9}Be in order to generate the Be^{-} beam necessary to measure the $^{9}Be/^{10}Be$ ratio by AMS. It is critical that the Be carrier contains as low an amount of ^{10}Be as

possible to avoid contaminating the sample. The Be carrier used at GU-SUERC is derived from a deep-mined beryl which yields very low ^{10}Be counts in the AMS. Following addition of a carefully measured amount of Be carrier the samples are digested in concentrated HF. The remaining solution then undergoes successive evaporations and re-dissolutions in the presence of hydrochloric acid (HCl) to completely eliminate fluorides until the final solution is a deep yellow-green colour. If any TiO is present (indicated by a powdery white precipitate) the samples require centrifuging to remove this. The samples are now ready to undergo anion exchange chromatography (AX) which separates Ti and Fe impurities from the sample. Some Ti (in the form of neutral species) does not get removed from the Be fraction using AX and it is removed using cation exchange chromatography (CX). During the CX the Be fraction is isolated. It is now precipitated as hydroxides at pH 8, washed and re-precipitated. After this stage the sample exists as hydroxide which is dried and then converted to beryllium oxide by baking at 800°C. The BeO samples are then mixed with niobium powder and pressed into copper cathodes ready for AMS analysis.

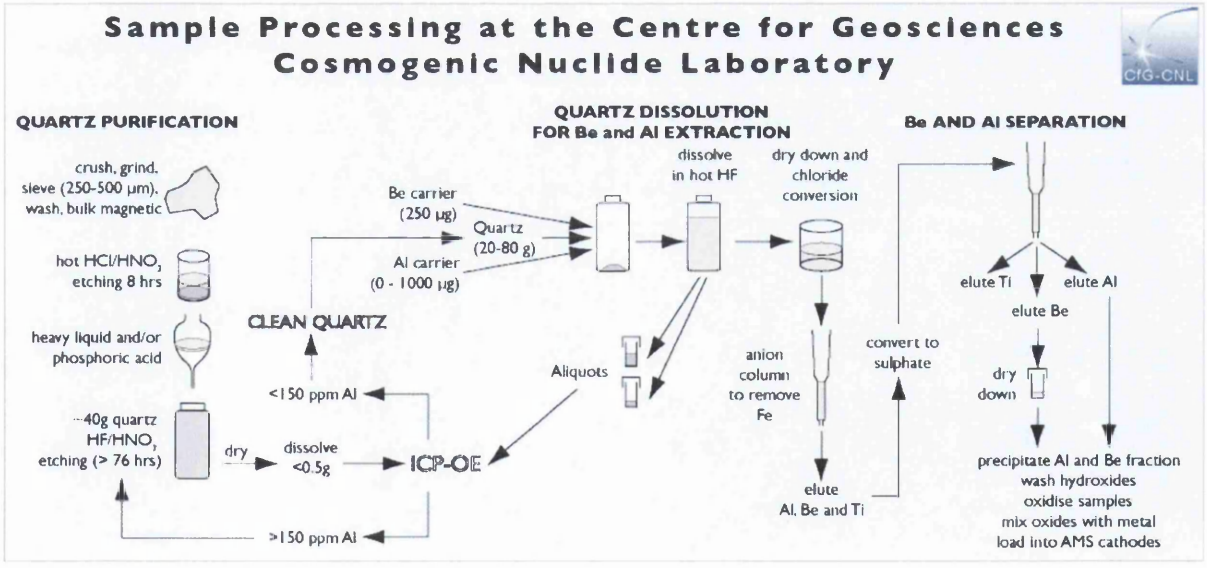

Figure 4.4 Stylised diagram showing the processes through which samples pass as they are prepared from AMS analysis.

Throughout the sample preparation great emphasis is placed on avoiding contamination of individual samples and cross contamination between samples. As the concentration of TCN's in samples is so low, any slight contamination will severely alter results. To check for contamination chemistry procedural blanks containing no samples but undergoing exactly the same chemical procedures are processed along with the samples. A full step by step guide to the sample preparation process can be found in Appendix 7.1.

5. Results and Discussion

5.1 Results

The sample location, shielding factors and production rates are shown in Table 5.1. , Chemical and AMS data, and the apparent exposure ages of the samples analysed in this study are shown in Table 5.2 and Figures 5.1 and 5.2

Table 5.1. Sample location, shielding factors and production rates.

Lab ID	Elev. (m)	Lat. (°N)	Long. (°W)	Shielding factor	Thickness* (corr. factor)	Peat thick. § (correction)	^{10}Be prod.rate† (atom g^{-1} yr^{-1})
GR0601	325	56.99	4.69	0.9976	3 (0.976)	0	6.73±0.58
GR0602	325	56.98	4.68	0.9811	3 (0.976)	0	6.62±0.57
GR0603	325	56.99	4.68	0.9269	3 (0.976)	0	6.25±0.54
GR0604	325	56.99	4.68	0.9543	3 (0.976)	0	6.44±0.56
GR0605	325	56.99	4.68	0.9715	5 (0.960)	50 (0.7431)	4.79±0.42
GR0606	250	56.99	4.72	0.9967	3 (0.976)	0	6.26±0.54
GR0607	240	56.99	4.73	0.9959	5 (0.960)	0	6.09±0.53
GR0608	220	56.97	4.74	0.9921	4 (0.968)	0	6.00±0.52
GR0609	220	56.97	4.74	0.9904	5 (0.960)	0	5.94±0.51

*Corrected using density = 2.65 g/cm^3 and an effective attenuation length of 160 g/cm^2
§ Corrected using density = 0.95 g/cm^3 and an effective attenuation length of 160 g/cm^2
† Sea level, high latitude ^{10}Be production rates taken as 4.96±0.45 atom g^{-1} yr^{-1} (Balco et al. submitted) scaled to site locations using Stone (2000).

Table 5.2. Sample chemical, AMS, and exposure age data.

Lab ID	Qtz (g)	Be Spike (µg)	^{10}Be/^{9}Be§ (x10^{-15})	^{10}Be/^{9}Be§ blank (x10^{-15})	[^{10}Be] (x10^4 atom g^{-1})	^{10}Be apparent exposure age (ka)∞
GR0601	20.903	253.9±5.1	124.00±4.86	3.73±0.91	9.76±0.46	14.2±1.4 (0.7)
GR0602	20.234	253.4±5.1	96.90±3.55	3.73±0.91	7.80±0.36	11.5±1.1 (0.5)
GR0603	21.325	253.7±5.1	95.10±3.38	3.73±0.91	7.26±0.33	11.3±1.1 (0.5)
GR0604	20.502	253.6±5.1	95.10±3.33	3.73±0.91	7.55±0.34	11.5±1.1 (0.5)
GR0605	19.099	253.6±5.1	63.10±5.58	2.7±0.81	5.36±0.52	10.8±1.4 (1.0)
GR0606	19.895	253.6±5.1	80.70±2.99	3.73±0.91	6.56±0.32	10.3±1.0 (0.5)
GR0607	13.288	253.7±5.1	56.50±6.85	2.7±0.81	6.86±0.90	11.0±1.7 (1.4)
GR0608	20.745	253.5±5.1	74.80±4.11	3.73±0.91	5.80±0.38	9.5±1.0 (0.6)
GR0609	20.851	253.3±5.1	77.30±4.02	3.73±0.91	5.97±0.37	9.8±1.0 (0.6)

§ ^{10}Be relative to NIST SRM 4325 with ^{10}Be/^{9}Be taken as 3.06x10^{-11}.
∞ ^{10}Be apparent exposure ages with full uncertainties and analytical uncertainties in brackets.

The exposure ages have been calculated using the scaling factors of Lal (1991)/Stone (2000) and the standardised SLHL production rate for ^{10}Be of 4.96 ± 0.45 atoms g^{-1} y^{-1} (Balco et al. submitted). The apparent exposure ages and external uncertainties obtained by using different scaling schemes are shown in Table 5.3 calculated using the CRONUS Earth exposure age calculator (http://hess.ess.washington.edu/math). It can be seen that the ages obtained by using the scaling schemes of Desilets *et al* (2003, 2006) and Dunai (2001) are slightly older than those obtained by using the factors of Lal (1991)/Stone (2000) (Table 5.3). The ages obtained by using the scaling scheme of Lifton *et al* (2005) are extremely close to the ages calculated using the scaling scheme of Lal (1991)/Stone (2000). However it should be noted that the ages obtained from all the available scaling schemes are statistically the same and that the results of this study are not particularly sensitive to the choice of scaling factors to be used. This is because the main difference between the various scaling schemes is in the way they deal with the varying effects of the Earth's magnetic field on production rates over time. At high latitudes the Earth's magnetic field is in the vertical direction and admits vertically incident radiation regardless of variations in overall field intensity (Section 2.2.2). Since the samples in this study are from relatively high latitudes all the scaling schemes produce similar ages.

Table 5.3. Apparent exposure ages with 1 sigma uncertainties from time-varying production models.

	Desilets et al. (2003, 2006)	Dunai (2001)	Lifton et al. (2005)	Lal (1991)/Stone (2000) – time dependent
GR0601	14.7±1.8	14.7±1.8	14.1±1.5	14.2±1.4
GR0602	11.9±1.5	11.9±1.5	11.5±1.2	11.5±1.4
GR0603	11.7±1.5	11.7±1.4	11.3±1.2	11.3±1.1
GR0604	11.9±1.5	11.9±1.5	11.4±1.2	11.5±1.1
GR0605	11.2±1.7	11.2±1.7	10.8±1.5	10.8±1.4
GR0606	10.6±1.3	10.6±1.3	10.2±1.1	10.3±1.0
GR0607	11.3±2.0	11.4±2.0	11.0±1.8	11.0±1.7
GR0608	9.7±1.3	9.8±1.3	9.4±1.1	9.5±1.0
GR0609	10.1±1.3	10.1±1.3	9.8±1.1	9.8±1.0

Figure 5.1 shows that all the samples, except for GR0601, overlap at two sigma external uncertainties. However, due to their proximity and hence the same scaling factors the apparent exposure ages can be compared using their internal uncertainties. The grouping of the ages from the 325m shoreline is particularly well defined as shown in figure 5.2. The ages of the samples from the two fan surfaces (Turret and Brunachan) are less well constrained and tend to be slightly younger. Using the analytical uncertainty only it can be seen that the samples from the Brunachan Fan are statistically younger than the other samples (Figure 5.2 and discussed in section 5.1.2).

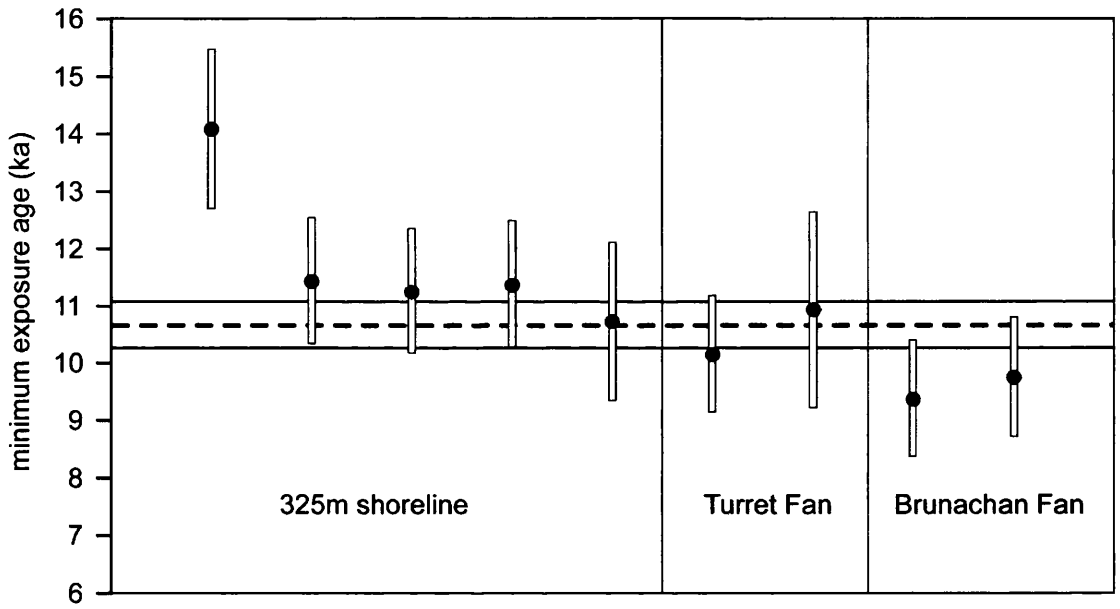

Figure 5.1. Glen Roy data with full uncertainty error bars. The dashed line is the weighted mean (10.7 ka) and the solid lines uncertainties (± 0.4ka) for all the data >12ka. The plot shows that for the full uncertainties all samples statistically overlap.

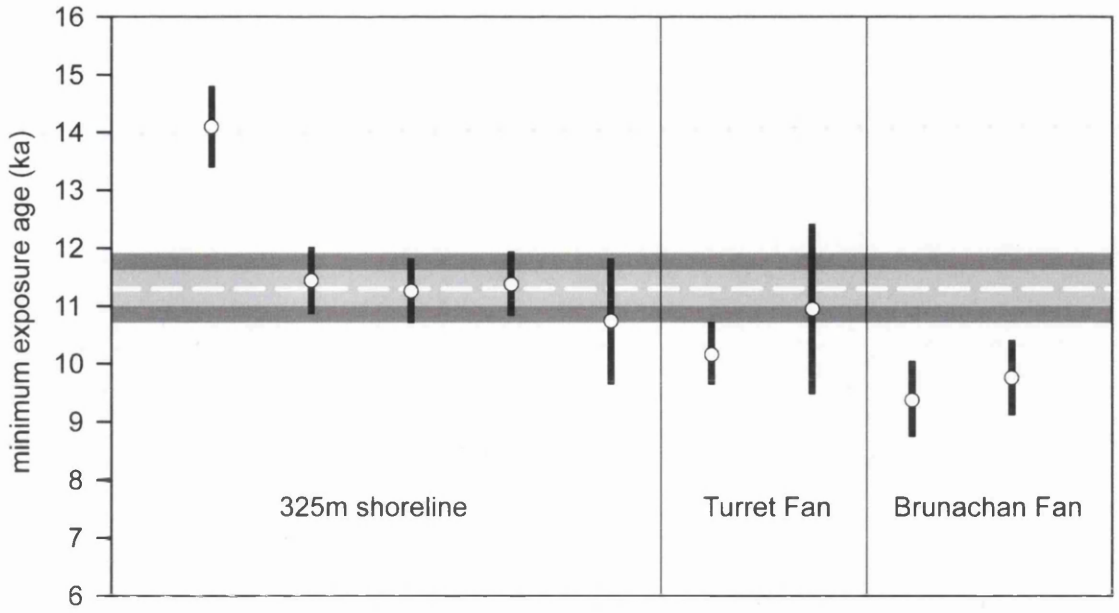

Figure 5.2. Glen Roy data with analytical uncertainty error bars. The white dashed line is the weighted mean (11.3 ka) for the 325m shoreline data <12ka. The light grey and dark grey boxes show the analytical and full weighted uncertainties. The plot shows that the Brunachan fan samples are statistically younger.

5.1.1 Interpretation of shoreline sample

The samples can be divided into two categories: samples collected from the 325m shoreline (GR0601-GR0605) and samples collected from the fan surfaces associated with the 260m shoreline (GR0606-GR0609). The ages of the samples from the 325m shoreline show excellent agreement with the exception of GR0601. This sample was collected from the outer edge of the shoreline and it is interpreted as not having had sufficient (<2m) amounts of overlying material removed during shoreline formation. Thus the exposure age of 14.2 ± 1.4 ka results from a TCN concentration that includes a component from the time following deglaciation after the Late Devensian Glacial Maximum (LGM) but before the formation of the shorelines. This age can be interpreted as a minimum age for deglaciation in upper Glen Roy following the LGM. How closely this age reflects the true deglaciation age depends on the amount of overlying material removed by shoreline formation and by erosion prior to and following this event. Since the exposure duration prior to shoreline formation is unknown the depth of material removed is not constrained except that it has to be less than 2m.

The other samples from the 325m shoreline all have ages that overlap at 1σ error. Taking a weighted mean of these ages gives an age of 11.3 ± 0.6 ka. This age is interpreted as representing the minimum age of formation of the 325m shoreline throughout Glen Roy. It is not possible to constrain the amount of erosion experienced by bedrock samples however it has been argued that frost action has been minimal since the end of the LLS (Sissons 1978). Thus it would be reasonable to conclude that the amount of erosion will be small. Nevertheless even a very low erosion rate of 1.5mm ka^{-1} would increase the apparent exposure ages by ~200yrs. Therefore it is important to note that the quoted age of the 325m shoreline is a minimum age.

Two lines of evidence support the interpretation that the exposure ages reflect the age of shoreline formation. Firstly samples were collected to minimise the likelihood of cosmogenic nuclide inheritance being significant. All shoreline sample sites were assessed by the method described in Section 4.1 in order to ascertain whether enough overlying material had been removed to reset the TCN signal. This was the case for all samples except GR0601, as discussed above. Thus the TCN concentrations in these samples are entirely the result of exposure following shoreline formation.

Secondly the exposure ages of samples from two different sections of the 325m shoreline (GR0602-GR0604 and GR0605 (Figure 5.2)) show good agreement. This indicates that the shoreline formed synchronously at these separate locations. It therefore seems reasonable to assume that shoreline formation was synchronous throughout Glen Roy and that the shoreline is not an inherited feature from an earlier glaciation. Therefore the exposure ages of the 325m samples are likely to reflect the age of formation of the entire shoreline and not just the age of formation of the sampled section(s).

5.1.2 Interpretation of fan samples

The apparent exposure ages of the four samples from the fan surfaces appear to cluster in two groups when compared using analytical uncertainties, with the two ages from the Turret Fan being slightly older than those from the Brunachan Fan (Figure 5.1 and 5.2). All the ages indicate that deposition was occurring on the fan surfaces into the Holocene. Given that the lakes are believed to have come into existence ~800y after the onset of GS-1 (12.65 cal yr B.P (Palmer *et al* 2007) and were in existence for ~550y (Palmer *et al* 2007) this shows that the fans were not abandoned until several hundred years after the 260m lake had drained.

The two samples from the Brunachan Fan show excellent agreement and are interpreted as indicating fan abandonment occurred at or after 9.6 ± 0.8 ka. The agreement shown between the 2 samples from the Turret Fan is not as good. However taking the large uncertainty associated with GR0607 into consideration the two ages are statistically in agreement. The weighted mean of these ages suggests that fan abandonment most likely occurred at or after 10.7 ± 0.9 ka.

It is necessary to make two basic assumptions in order to interpret the ages of the fan samples as reflecting the time of fan abandonment. Firstly, that the erosion and sedimentation processes responsible for the emplacement of the sampled clasts were sufficiently rapid to minimise TCN accumulation before or during emplacement. Secondly that erosion since fan abandonment (and hence loss of ^{10}Be) has been negligible, i.e. the ^{10}Be concentration in surficial clasts is entirely the result of accumulation in the period post dating fan abandonment.

These two assumptions can be supported on the basis of several lines of evidence. With respect to the first assumption, and realising there are only four samples, the absence of ages

older than the 325m shoreline supports rapid erosion and emplacement of the clasts. If the clast material had been residing at the surface for any significant period of time before erosion it might be expected that they would yield exposure ages predating the 325m shoreline. However given the fact that we are attempting to resolve between events seperated by <1ka, even short exposures at the surface before erosion and emplacement would be significant. Thus ages must be treated as maximum ages of fan abandonment.

Absence of significant erosion since deposition is assumed due to the fact that the clasts are derived from relatively hard lithologies and that it is thought that frost shattering has been insignificant since the formation of the roads (Sissons 1978). As the importance of any slight erosion of the clasts is much less than the importance of any prior exposure in terms of contributing to the TCN signal the exposure ages are still considered maximum ages for fan abandonment. However the exposure ages of all the fan samples are minimum exposure ages as they all assume that there has been zero erosion of the sampled clasts during the time of exposure. If any erosion has occurred then the quoted ages will under estimate the true length of time that the clasts have been exposed for and thus the maximum age of fan abandonment is potentially older than indicated by the exposure ages.

The ages obtained from the surfaces of the fans indicate that the Turret fan was abandoned before the Brunachan Fan. If the fans were abandoned due to knickpoint propagation as a result of the base level fall associated with lake drainage then it would be expected that the downstream (Brunachan) fan would have been abandoned first.

This discrepancy may be explained by considering the differences in morphology of the two fans. The Brunachan Fan is small and very steep in comparison to the larger, flatter Turret Fan. From the point where the fan begins the Palaeo-River Turret would have had to transport material over 1km across a flat gradient to reach the sample sites. In comparison the Palaeo-Allt Brunachan would have only had to transport material a few hundred metres

across a steep faced fan to deposit at the sample sites. It is possible that following lake level fall the Turret was unable to transport material as far as the sample sites whereas the Brunachan (especially in times of peak flow) could. Thus little or no deposition occurred on the outer portion of the Turret Fan while deposition was still occurring across the whole of the Brunachan fan. This would result in older ages for samples from the surface of the Turret Fan.

Alternatively landsliding could have emplaced material on the Brunachan Fan. This emplaced material could have an apparent exposure age that is considerably younger than the age of fan abandonment, thus explaining why the ages indicate that the Brunachan Fan appears to have been abandoned after the Turret Fan. The sampling strategy was designed to minimise this possibility. However the closeness of steep slopes to the Brunachan Fan coupled with the steep nature of the fan mean that landsliding cannot be ruled out as a complicating factor.

5.2 Discussion

5.2.1 Rates of shoreline formation

The close agreement of the exposure ages of samples GR0602-GR0605 is taken to indicate synchronous shoreline formation throughout Glen Roy. If this assumption is extended to all 3 shorelines then there are implications for the rates of shoreline formation. Synchronous formation implies that the shorelines are not partly inherited features and were formed entirely during the LLS. This means that the time available for shoreline formation is limited by the length of time for which the lakes existed at any given level during the LLS. Palmer *et al* (2007) linked the varve sequence in Glen Roy to the GRIP ice core record and indicated that these varves were deposited during the LLS. Further analysis of these varves

has shown that the 325m lake existed for 137 years during the rising sequence and 66 years during the falling sequence. Therefore the entire 325m shoreline must have formed in a minimum of 60 years and a maximum of 203years. Similarly the top (350m) shoreline formed within 137 years and the 260m shoreline within 185 years (Palmer pers. comm.).

In the time available for formation of the 325m and 350m shorelines features with average widths of 10.5m and 10.4m respectively developed (Sissons 1978). The shorelines in Glen Roy are not unique examples of rapid shoreline formation. Dawson *et al* (1987) report shorelines up to 5.3m wide cut in bedrock in the space of 75-125 years around a formerly ice dammed lake in Norway. The calculated rates of shoreline widening were 4.2-7.1 cm yr^{-1}. Table 5.6 shows the equivalent rates of shoreline widening for the Glen Roy shorelines using Palmers varve data to constrain the time available for shoreline formation as well as rates from other examples of rapid cold climate shoreline formation.

Table 5.6 Showing the comparable rates of shoreline widening for a variety of cold climate shorelines. It can be seen that the rates implied for the Glen Roy shorelines are comparable to the rates from the other examples.

Shoreline	Time available for formation (yr)	Width (m)	Rate of widening (cm/yr)
325m Glen Roy (min time)	60	10.5	17.5
(max time)	203	10.5	5.17
350m Glen Roy	137	10.4	7.59
Norwegian Shorelines (Dawson *et al* 87) (min time)	75	5.3	7.07
(max time)	125	5.3	4.24
Main Late Glacial Shoreline [MLGS] (Dawson 88, Stone *et al* 96)	1500	50	3.33
MLGS (max width)	1500	150	10.00
Lake Bonneville, USA (Oviatt *et al* 92, Oviatt 97)	500	75	15.00

While these rates are higher than those reported by Dawson *et al* (1987) the lake that existed in Glen Roy was significantly larger than that associated with the Norwegian shorelines (Dawson *et al* 1987). It is conceivable that the longer fetch available in the Glen

Roy lake meant wave action was more significant and was responsible for the higher rates although this effect would be limited to the sections of shoreline exposed to the prevailing wind direction. Alternatively it may be that the LLS climate was more conducive to significant frost action than the prevailing climatic conditions at the time of the formation of the Norwegian shorelines leading to higher rates of shoreline widening in Glen Roy.

Further examples of significant shorelines cut in a short time are those of the Main Late Glacial Shoreline (MLGS) in Scotland and the shorelines of pluvial Lake Bonneville in the Western United States. Stone *et al* (1996) showed that the MLGS formed entirely during the LLS. The MLGS is typically 50-150m wide (Dawson 1988). Formation of this size of shoreline in the short (~1500y) timescale of the LLS implies rapid rates of shoreline widening. Assuming that the MLGS had the entire LLS to form the rates of shoreline widening involved are comparable to those at Glen Roy (Table 5.6). While the MLGS is a marine platform it occurs in many enclosed sea lochs and other places where the fetch is limited and thus wave action would not be any more significant than in the Glen Roy lake. Indeed to explain formation of the MLGS during the LLS Stone *et al* (1996) invoke many of the processes, such as frost heaving and ice push, that are used to explain the formation of the parallel roads of Glen Roy and other lake shorelines in cold climates (e.g. Dawson *et al* 1987, Sissons 1978, Dionne 1979).

Schofield *et al* (2004) report erosional platforms 75m wide that form part of the Bonneville shoreline of Pleistocene lake Bonneville. As the lake level was at the level of the Bonneville shoreline for ~500 yr (Oviatt *et al* 1992, Oviatt 1997) this implies average rates of shoreline widening of ~15 cm yr^{-1}, comparable to the highest possible rates in Glen Roy.

These examples along with Glen Roy, show that rapid shoreline formation is a widely occurring phenomenon especially where cold climatic conditions cause frost action to be significant. This evidence supports the interpretation of the Glen Roy shorelines as being

exclusively LLS features as there was ample time available at each of the lake level still stands for the shorelines to be developed.

5.2.2 Timing of LLS maximum ice extent

The interpretation of the weighted mean age of the 325m samples as being the minimum age of formation of the 325m shoreline has implications for the timing of maximum LLS ice extent in Scotland. The ice margin associated with formation of this shoreline lies close to the maximum extent of LLS ice in Glen Roy (Sissons 1978). This would suggest that ice was at this location very soon before and after it reached its maximum extent. This is supported by varve data that shows that ice only extended beyond this point for 137 yrs, the time for which the 350m lake existed (Palmer pers.comm.). Thus the 325m shoreline must have been formed at a time just before or after ice in Glen Roy reached its maximum extent.

Ice in Glen Roy was sourced from the same areas as the majority of the main Scottish ice cap during the LLS, to the South and West of the Great Glen (Peacock 1970, Sissons 1979a). As it shared the same source areas it seems logical to conclude that the ice occupying Glen Roy reached its maxima synchronously with the rest of the LLS ice cap. Taking these two conclusions together, the 325m shoreline formed at a time closely equating to the time of the maximum extent of LLS ice in Scotland. Therefore it can be argued LLS ice in Scotland reached its maximum extent at a time near to 11.3 ± 0.6 ka. Taking this date as equating to the time of the maximum ice extent puts the LLS maxima outwith GS-1 as defined by Björck *et al* (1998), 12.65-11.5 GRIP yr B.P. It would therefore seem likely that the formation of the 325m shoreline occurred soon after the LLS ice began retreating from its maximum extent.

Varve data from the lake deposits in Glen Roy suggests that the LLS ice sheet in Scotland reached its maxima ca. 840y after the onset of GS-1 (Palmer *et al* 2007). This agrees well with the conclusion that the age of the 325m shoreline closely follows the time of maximum LLS ice extent. The data from Glen Roy would indicate that the LLS ice cap reached its maximum extent late in GS-1 and that a significant amount of ice was in existence into the early Holocene. Evidence from elsewhere in Scotland also points to a LLS maximum towards the latter end of the stadial. Two quartzite boulders from a recessional moraine in Assynt, northwest Scotland, have ^{10}Be exposure ages of 10.1 ± 1.0 ka and 11.2 ± 1.0 ka (Bradwell 2006). This indicates that ice in this area was retreating from a maximum during the early Holocene. It could be suggested that this supports the argument that the LLS maximum was late in GS-1 although there is the possibility that the growth and retreat of the glacier associated with this moraine was significantly asynchronous with the rest of the Scottish ice cap.

Although the LLS in Scotland is roughly equivalent to GRIP event GS-1 (12.65-11.5 GRIP yr B.P) it is often assigned an age of 12.9-11.5 Cal yr B.P (e.g. Benn & Ballantyne 2005, Hubbard 1999, Ballantyne 2002). This would equate the LLS to GRIP events GI-1a and GS-1 (Björck *et al* 1998). There were cooling events at 12.9 ka and 12.65 ka (Lowe *et al* 1999, Mayle *et al* 1999) and it is important to determine which of these was critical for initiation of glaciation in Scotland. Hubbard's (1999) numerical model suggests that LLS ice in Scotland could have reaches its maximum extent after ca. 550 years. It would seem easiest to reconcile this with the data from Glen Roy if glaciation was initiated by the cooling event at 12.65 cal. yr B.P which marks the start of GS-1 rather than the event at 12.9 cal. yr B.P which marks the onset of GI-1a.

The suggestion that the cooling at 12.65 ka Cal. yr B.P was responsible for initiation of ice cap growth in Scotland is very tentative. Much more work needs to be done both in

terms of collecting field evidence and numerical modelling in order to further support or refute this suggestion. However what this data does strongly suggest is that significant amounts of ice survived into the early Holocene, not just in the high corries but also forming valley glaciers at lower elevations. More work remains to be done in order to constrain the rates at which this ice disappeared following the climatic amelioration that marks the end of GS-1.

5.2.3 Timing of Fan and 260m shoreline Formation

Of the more recent work published on Glen Roy and the parallel roads there has been much debate regarding the age of the alluvial (Brunachan & Reinich) and fluvio-glacial (Turret) fans in upper Glen Roy. Sissons & Cornish (1983) propose that they are entirely LLS features deposited into the lowest (260m) lake level, a view supported by Lowe & Cairns (1991). Alternatively Peacock (1986) argues that these features were formed prior to the establishment of an ice-dammed lake in Glen Roy, namely that they are Late Devensian in age.

None of the ages obtained from the fan surfaces pre-dates the LLS. This would tend to suggest that at least the upper portions of the fans were deposited during and just after the LLS. The ages do not support the theory that the fans were formed entirely prior to the initial damming of a lake in Glen Roy. If this was the case it could be expected that the exposure ages of the samples would pre-date the LLS.

It cannot be ruled out that the fans were partially deposited prior to the LLS with subsequent deposition occurring during and after this time. This would account for the exposure ages on the surfaces of the fans. However the simplest explanation is that the features were predominantly deposited during the LLS with some deposition on the

uppermost surfaces occurring during the early Holocene, much in accordance with the views of Sissons & Cornish (1983).

Inferring the time of development of the 260m shoreline from the exposure ages of the fan samples is not simple as these ages do not directly measure the time of shoreline formation. However they can be used to constrain the time of shoreline formation. It is generally considered that the 260m shoreline formed at the time the lake was at this level on the falling limb of the lake sequence. This is because then 260m shoreline does not show seismically displaced sections in areas where the upper shorelines do (Dawson *et al* 2002), thus it is concluded that the 260m shoreline formed after the upper shorelines. Material deposited onto the fan surfaces before the formation of the 260m shoreline, while the lake existed at a higher level, would have been shielded by tens of metres of water. This water would have reduced TCN production to effectively zero. As a result any material deposited on the fan surfaces while the lake was standing at a higher level would have only began accumulating TCN's when the lake level fell below 260m, after the 260m shoreline had formed. Similarly any material subsequently deposited on the fan surfaces, by floods or landslide, would also post-date shoreline formation.

It is therefore reasonable to argue that formation of the 260m shoreline pre-dates the abandonment of the fans. Definitively dating the time of its formation is not possible with the samples analysed in this study. Given the short lived nature of the lakes, it is expected that the 260m shoreline would have formed shortly after the 325m shoreline. Thus the ages from the Turret Fan, being closer to the age of the 325m shoreline, may more closely reflect the age of the 260m shoreline. Taking the youngest of these ages, it seems reasonable to conclude that the 260m shoreline must have formed before 10.3 ± 1.0 ka and it is possible that the age of the other sample (11.0 ± 1.7 ka) closely reflects the time of formation of the

260m shoreline. However it is not possible to state this with certainty given the limited number of ages available and the large uncertainties associated with these samples.

5.2.4 Palaeoseismicity

Following deglaciation of the Devensian ice sheet Scotland has undergone glacio-isostatic uplift (Firth & Stewart 2000). Associated with this uplift have been numerous seismic events that have resulted in deformation structures being preserved in soft sediments (Davenport & Ringrose 1987, Ringrose 1989a) and shoreline displacement (Ringrose 1989b, Sissons & Cornish 1982). It has been shown that the majority of these events were confined to the time of deglaciation and the early Holocene (Firth & Stewart 2000). However it has not been possible to constrain the precise timing of any given seismic event.

The dates obtained in this study provide an opportunity to constrain the seismic event that was responsible for this displacement. As the event displaced the 325m shoreline it must have occurred after the time of the shorelines formation. Thus using the ^{10}Be dates from this shoreline it is possible to say that the seismic event occurred after 11.3 ± 0.6 ka. This age helps constrain the occurrence of what is to date the largest known post-glacial seismic event reported from Scotland (Ringrose 1989a). It supports the conclusion of Firth & Stewart (2000) that post-glacial seismicity was most pronounced during the early Holocene.

6. Conclusion

The use of cosmogenic nuclide exposure dating provides an opportunity to obtain independent age control on the timing of the formation of the "parallel roads" of Glen Roy. Obtaining such age control using other dating techniques (e.g. ^{14}C & OSL) has, thus far, proved impossible. Knowledge of the exact timing of the "parallel roads" helps us understand the evolution of the landscape in response to ice damming of the drainage system. It also allows us insights into the glacial history of the region.

The ages published in this study support the long held view that the "parallel roads" are Loch Lomond Stadial (LLS) features. Even though the minimum age of the 325m shoreline (11.3 ± 0.6 ka) falls just outwith the limits of the LLS (12.9-11.5 cal yr B.P) an erosion rate of >1.5mm ka^{-1} on bedrock samples since exposure would increase the apparent exposure ages by > 200 years. This would increase the age of the shoreline to within the LLS limits. The consistency of the shoreline sample ages suggests synchronous formation of this shoreline. The minimum ages of the fan samples lie outwith the lower LLS age limit and suggest that deposition was occurring on the fan surfaces into the Holocene. This precludes the suggestion that the Brunachan and Turret fans are entirely pre-LLS features (Peacock 1986).

The ^{10}Be ages from the "parallel roads" are some of the first cosmogenic nuclide dates relating to the LLS in Scotland. The date obtained from the 325m shoreline suggests that the time of maximum ice extent was towards the end of GS-1. This raises the question of which one of the known climatic deteriorations (at 12.9 cal yr BP and 12.65 cal yr BP) was responsible for the initiation (or acceleration) of ice cap growth. Knowledge of this could help us understand the sensitivity of Scotland's climate at this time to external forcing such

as a slowdown of the North Atlantic Thermohaline Circulation (Clark *et al* 2002). This understanding could prove useful for attempts to model future climatic scenarios. Investigation of this question requires many more dates relating to the LLS, this study provides some of the first such dates.

7. Appendices

7.1 Sample preparation - step by step

Quartz Cleaning

Summary

For preparing very pure quartz separates...

Most silicate minerals dissolve faster than quartz in dilute HF and can be etched away to leave a very pure quartz residue. Some quartz is lost - usually ~10% of coarse-grained fractions (500-850 □m) and up to 20-30% of fine-grained fractions (250-500□m). It is difficult to get good yields from this procedure using grain sizes <250 □m.

The HF leach has the added advantage of dissolving the outermost shell of the quartz grains, as well as etching cracks, where any contamination by meteoric ^{10}Be would be concentrated.

Some minerals will not dissolve (e.g. garnet, zircon, rutile, ilmenite). Fortunately, except for garnet, these are trace constituents of most rocks. Muscovite is the only other common mineral that causes problems. It dissolves at about the same rate as quartz, so the procedure won't concentrate quartz relative to muscovite.

Several techniques are available to remove interfering minerals.

- Magnetic separation can be used to remove most magnetic minerals. Quartz and feldspar are not magnetic and can not be separated in this manner.
- An initial heavy liquid separation will remove garnet and muscovite (as well as most other mafic silicates and oxide minerals), if present. Heavy liquid separation will not result in complete removal of feldspar from the sample.
- Froth floatation techniques may be more useful. Froth floatation is the most rapid method for removing feldspar and mica from the sample.
- Digestion in phosphoric acid will remove aluminosilicates very efficiently, however it is time consuming and expensive.

Not all rocks need to be processed beyond a HNO_3/HCl leach before HF treatment. Small amounts of zircon, ilmenite, etc. in the final sample do not cause problems in the subsequent Al-Be extraction chemistry.

Sample crushing, milling, sieving and washing

For cosmogenic nuclide dating we require pure quartz with a grainsize of 200 – 500μm. Samples are usually in the form of rocks that consist of many minerals. The aim of the physical disintegration of the samples is to permit extraction of quartz from among the other minerals.

Procedure

In the rock crushing lab (basement of the Gregory Building), and wearing a dust mask and safety glasses…

1. Turn on the dust extraction system.
2. Make sure the jaw crusher, grinding mill, and sieves are clean.
3. reduce the sample to <1 cm chunks with the jaw crusher
4. feed the crushed material into the grinding mill
5. separate the sample into 3 size classes: >500μm, 250-500μm and <250μm using the designated stack of sieves. If there is not enough 250-500μm material repeat step 2 with the >500μm fraction.
6. Transfer the >500μm and <250μm size fractions into labelled plastic bags.
7. Place the 250-500μm fraction into a cleaned aluminium dish and rinse out the very fine materials, taking care not to loose the coarser sample material. Continue rinsing until the rinse water remains clear.
8. EITHER place the aluminium dish into the drying oven, OR transfer about 100g of the wet sample into a 600ml glass beaker for further processing in the Geochemistry Lab.
9. Clean the jaw crusher and grinding mill.
10. Carefully clean the sieves, making sure no grains remain in them.

HCl/HNO_3 leaching to remove carbonates and metals

Pre-clean samples in hot 10% HNO_3. All carbonates must be removed before reacting the samples with HF.

Procedure

For samples brought directly to the Geochem. Lab from the Rock Crushing Lab the first 2 steps can be omitted.

1. Pour about 100 grams of sample into a glass beaker.
2. Wash the sample with water to remove the remaining fines.

3. Under the fume hood and wearing gloves add enough 10% HCl/HNO_3 to cover the sample.
4. Place the beaker on a hotplate on **LOW** setting and cover it with a watch glass. **Do not heat the sample too vigorously**. Leave the sample overnight.
5. Cool the beaker and carefully pour the acid into the hazardous waste container without loosing sample.
6. Rinse the sample several times with water and discard the liquid into the hazardous waste container.
7. Once the rinse solution is clean dry the sample in the drying oven.

Magnetic separation

Separate magnetic minerals using the Frantz Magnetic Separator in the Mineral Separation Lab.

Procedure

1. Turn on the magnetic separator
2. Set the magnetic field strength to 0.1 A.
3. Pour the sample into the hopper.
4. Collect the magnetic and non-magnetic fractions.
5. Turn off the magnetic separator and clean it.
6. Turn the magnetic separator on again and set the magnetic field strength to 0.5 mA.
7. Repeat the magnetic separation using only the non-magnetic fraction derived from Step 4.
8. Set the magnetic field strength to maximum.
9. Repeat the magnetic separation using only the non-magnetic fraction derived from Step 7.
10. Turn off the magnetic separator and clean it.
11. EITHER transfer the separated fractions into labelled plastic bags, OR pour the non-magnetic fraction into a labelled 500ml polyethylene (PE) bottle for treatment by HF leaching

HF leaching to remove feldspar and remove meteoric ^{10}Be

Most silicate minerals dissolve faster than quartz in dilute HF and can be etched away to leave a very pure quartz residue. Some quartz is lost - usually ~10% of coarse-grained fractions (500-850 □m) and up to 20-30% of fine-grained fractions (250-500□m). It is difficult to get good yields from this procedure using grain sizes <250 □m.

The HF leach has the added advantage of dissolving the outermost shell of the quartz grains, as well as etching cracks, where any contamination by meteoric ^{10}Be would be concentrated.

Procedure

HF leaching

1. Label a clean 500 ml polypropylene (PP) bottle with the sample name or number.
2. Transfer ~60g of the sample to the bottle.
3. In the fume hood make up a ~2% HF solution in the 2.5 liter container (2500ml H_2O + 50ml HF).
4. Fill the sample bottle with the 2% HF solution to within 2 cm of the top.
5. Gently squeeze the bottle before capping. This gives the contents room to expand when the bottle heats up. Also, loss of vacuum will alert you to the possibility that the bottle has leaked. Check that the bottle is tightly sealed and holding its slight vacuum.
6. In the fume hood, gently invert it 3-4 times to mix the contents.
7. Mark the bottle to indicate how many times it has been processed.
8. Place the bottle in the ultrasonic bath for 72 hours. Shake the bottle several times during sonication.

After the first 3-days, change the HF as follows.

9. Cool the bottles (if they are warm).
10. In the fume hood, uncap the bottle and discard the solution into the HF waste container. Be careful not to pour out the sample.
11. Rinse the remaining grains thoroughly with 3 changes of MilliQ (18.2 MΩ) water, decanting off the rinse water into the waste acid container while any clay or fine, milky fluoride precipitate is still suspended, but after "fine sand"-sized grains have settled. Don't worry about losing some of the very fine grains, unless the sample is unusually small.
12. Add 2% HF solution to the bottle just like in the first treatment and repeat the 3-day processing for a second time.
13. Repeat the process for a third time.

Sample recovery

Pure quartz samples have a uniform appearance and do not cake on the floor of the bottle.

Impure samples usually appear speckled and may contain a cloudy fluoride precipitate.

If the sample does not appear pure, repeat the HF leaching for another 3-day period.

If the sample appears pure, recover the sample:

Cool the bottle.

1. In the fume hood, uncap the bottle and discard the solution into the HF waste container.
2. Rinse with at least 6-8 changes of MilliQ as above. Try to rinse away any trace of milky fluoride. The rinse water must be clear (and absolutely free of residual HF).
3. Dry in the oven.
4. Cool the samples and transfer them to a labelled ziplock bags.

Aluminium Determination from a Mineral Aliquot (MA)

To assess the purity of the quartz we determine the aluminium content of the cleaned separate. It is essential to obtain the lowest possible Al concentration. The higher the Al concentration, the lower the $^{26}Al/^{27}Al$ ratio for measurement, the fewer ^{26}Al nuclides counted and the worse the counting statistics. The Al concentration should preferably be in the range 10 - 100 ppm. A higher concentration generally (though not always) indicates the presence of an impurity such as feldspar, muscovite or an insoluble fluoride residue from the quartz clean-up (e.g. Na_3AlF_6). Note that ~0.5% feldspar gives ~1000 ppm Al.

Procedure

Static charge should always be removed before weighing.

1. Label and weigh a 15 ml Teflon round-bottom vial and lid on the 4-figure balance. Record the tare weight to 4 decimal places on the sample data sheet. Using a stainless steel spatula, transfer 0.3 - 0.6 g of the sample into the vial. Replace the lid and record the weight. The amount of sample is not too critical, but its weight must be recorded accurately. Be careful when replacing the lid, as static charge may cause small grains to jump up onto the lid or out of the vial. Clean the spatula with a kimwipe (±ethanol) before using it for the next sample.
2. When all the samples have been weighed into vials, open the vials in an HF-rated fume hood and add approximately 10 ml of conc. HF (40 - 50% w/w, ~30 M) and 1 – 2 drops of 1:1 H_2SO_4.
3. In the fume hood, cap the vials and leave them standing overnight to allow the quartz to dissolve.
4. In the fume hood, place the open vials on the hotplate at 120°C. Keep track of which lid belongs to which vial. Fume off HF/H_2SO_4. Do not overheat the small flat-bottomed vials, as solutions will boil and damage the hotplate surface. Because H_2SO_4 has a higher boiling point than HF you will be left with a golden-brown drop of material containing a few hundred μg total of Al, Fe and Ti fluorides.
5. If any quartz remains (usually only if the original sample was very coarse-grained), ***cool the vials*** and repeat the procedure from step 2 with a further 2 - 3 ml of HF and 1 drop of 1:1 H_2SO_4.
6. Cool the vials. Dissolve the dry residue in 8 ml of 2% HNO_3 (use the Eppendorf 1-5 ml adjustable pipettor and the attachment dedicated to dilute HNO_3). Cap the vials with their original caps and leave to stand (preferably overnight). The fluorides should dissolve totally to give a clear (or perhaps faintly green) solution.
7. Invert the capped vials a few times to homogenise the solutions, then weigh and record the vial+solution weights.
8. Decant the solutions into labelled centrifuge tubes for AAS or ICP analysis.

Clean the Teflon ware using the procedure outlined in General Lab Practice.

Carrier Addition and Sample Digestion

Our aim is to extract Beryllium from the quartz sample and to measure the $^{10}Be/^{9}Be$ ratio using AMS. However, Be is a very rare element in quartz. Therefore it is necessary to spike the sample with a known quantity of ^{9}Be. The aim of spiking is that we can trace the movement of the Be through the processing and that the very low concentrations of naturally occurring Be will follow the same path as the added Be. Also need to end up with enough Be to generate an ion beam in the AMS. Obviously we do not want to introduce ^{10}Be to the sample since this is the nuclide we are trying to measure. For this reason we have Be carrier solutions with known concentrations of ^{9}Be. It is critical that a low-level carrier is used for samples with potentially low levels of ^{9}Be.

The amount of sample required for the AMS measurement of ^{26}Al is a minimum of 1 mg, but larger amounts are easier to run. For samples containing 50 ppm Al, at least 20 g of quartz should be dissolved, but note that processing more than 40 g becomes unwieldy; 20g should be enough unless sample is quite young (~25 g of sample should be processed in that case). In some samples the Al concentration is so low that it needs to be spiked with Al carrier. We aim to have a total of 1000-1500ug Al on each sample. If the sample has less Al, add carrier to reach this value but never spike with more than 1000ug of Al. For blanks, add 2ml of 1000ppm Al carrier solution. To add Al carrier solution to samples use the same procedure as for the Be carrier.

Procedure

Sample weighing

1. Label, remove static (by wrapping bottle in foil paper or using the anti static cathode) and weigh a clean FEP Teflon bottle (bottle+lid). Make sure to use a bottle (250 or 500ml) large enough to contain the HF (~5ml per gram of sample). Record the tare weight on the sample data sheet. Transfer the sample to the bottle. This is best done with the help of a funnel (one per sample). It helps to reduce static if bottle is wrapped in foil paper when transferring the sample. Some grains will charge and cling to the bottle walls. No problem. Cap the bottle.
2. Remove static and re-weigh. Subtract the bottle tare to determine the sample weight.

Be carrier addition (to add 250-300ug of Be to all samples including the blank 1ml of TCW Be carrier-)

1. Take the current Be carrier bottle, invert it a few times to homogenize the solution. Be sure drops of condensation around the lid are mixed in. Remove static (by wrapping

bottle in foil paper or using the anti static cathode) and weigh it. Record the initial weight in the blank sample log sheet (and if possible, confirm that it equals the final weight from its last use).

2. Load the 1000 µl Eppendorf pipette with a clean tip and uptake 820µl of Be carrier. Be sure the tip does not touch anything while handling the pipette. If the tip does touch something, discard it and take another. Start the Be carrier addition with the blank sample of the batch. Open the sample bottle.
3. Tare the balance to zero. Remove the carrier, open it and pipette carrier into the sample bottle. Eject the carrier smoothly, being sure not to leave a drop in the tip. If this happens uptake MQ water and dispense over the sample to ensure ALL carrier is added. Don't allow the tip to touch the sample bottle. Recap the carrier bottle as quickly as possible, remove static and re-weigh it. The balance will read the weight removed. Record the weight and the Be concentration of the carrier. Calculate the Be added.
4. Repeat the process from point 3 until Be carrier is added to all samples.
5. At the end of each session tare the balance to zero and record the final weight of the carrier bottle in the blank log sheet for cross-checking. Check that the cap is screwed on firmly and seal it with parafilm.

Sample digestion

1. In fume hood, wearing gloves and goggles....Using the measuring cylinder marked for concentrated HF, add 5ml AR grade HF for each gram of quartz in the sample bottle. Add ~100ml HF (c) to the blank bottle.
2. Cap the bottle, tighten the lid down, then back it off ~1/4 turn. The bottle must not be gas-tight (check by squeezing it gently). **Beware if the sample is fine-grained** – the reaction may proceed fast and the bottle may get very hot. If it looks like starting to boil, be prepared to sit it in a beaker or basin of cold water to quench the reaction a bit. Don't swirl the bottle at first – the initial reaction doesn't need any encouragement. **Never shake the bottle!**
3. Once the reaction has subsided (usually 1-2 hours), the bottles can be placed around the edges of the hotplate set on a low temperature (set 2, ~50°C). They only need very gentle warming to ensure overnight dissolution. From this point on, they can also be swirled occasionally to mix HF down into the dense H_2SiF_6 forming around the quartz grains (remember to close the lid tightly before swirling sample). During the day the temperature can be increased slightly (SET 3, ~ 100 °C)
4. Once all the quartz has been dissolved turn off the hotplate and cool the bottles to room temperature. The time required for dissolution varies depending on sample. 30 g of pure quartz may take up to 3 days; 60 g may take 4 days. If solution seems to be saturated (dissolution goes very slowly) add more HF(c) to sample. (If brown-black grains are present in solution and do not dissolve after adding more HF; heating and swirling samples for a long period of time they are probably not quartz. Make a note of it and carry on with sample preparation as indicated in point 5).
5. Tighten the caps, being wary of any droplets of condensation inside the screw threads that might be squeezed out onto the surface of the bottle.

Splitting for Aluminium Determination

Accelerator mass spectrometry does not provide absolute values of nuclide concentrations in the sample. Rather AMS provides a ratio between the cosmogenic nuclide and the stable nuclide occurring in the sample but not produced by cosmic ray interaction. For example, AMS gives us the $^{26}Al/^{27}Al$ ratio, where ^{26}Al is the cosmogenic nuclide and ^{27}Al the stable, native aluminium in the sample. Therefore, to determine the actual concentration of cosmogenic ^{26}Al in the sample we need to know the ^{27}Al concentration in the sample. Because cosmogenic ^{26}Al is so rare we can estimate the stable ^{27}Al concentration by measuring the total Al in the sample solution (parent solution). Total Al in an aliquot of the parent solution is measured by ICP.

Procedure

1. Homogenize the solutions by swirling and inverting the bottles to mix in HF condensed around the top of the bottle. Total sample Al concentrations will be determined from splits (aliquots) of these solutions, so they must be thoroughly mixed.
2. Weigh the bottles. For all but the smallest samples it will be necessary to use the top-loading balance (accurate to 3 decimal places). Subtract the bottle tare weight and calculate the total solution weight.
3. For each sample calculate the expected Al concentration (ppm) of the parent solution and use this to calculate the amount of parent solution required to obtain a ~10 ml ICP solution with ~7 ppm Al.
4. For each sample, take a Teflon vial. Label, remove static, weigh the vial and record the weight on the sample data sheet.
5. In the fume hood; open the vials; open the sample bottle. Using a disposable pipette transfer the calculated amount of parent solution into each vial. Remember you are transferring HF. The actual amount transferred doesn't matter too much provided is close to the calculated amount. Do not try to pour solution back into the parent solution bottle.
6. Without rushing, but as quickly as possible, close the vials. Weigh them and record the weights. Calculate the weight of each split. Take care not to splash any of the split solutions onto the lids of their vials when transferring them to the balance.
7. After splitting each sample, the aliquots can be dried down to remove HF in preparation for ICP analysis. Transfer aliquots back to the fume hood, taking care not to splash liquid into the lids of the vials. Add 5-10 drops of 1: 1 H_2SO_4 to each and dry at setting 4 (~90°C-140°C) on the hotplate (OK to leave overnight at set 3 ½ - 4). A small dot of liquid or a precipitate of Fe-Al-Be-Ti alkali salts should appear in the base of each vial after evaporation.
8. Cool the vials. Dissolve the dry residue in 10 ml of 2% HNO_3 (use the Eppendorf 1-5 ml adjustable pipettor and the attachment dedicated to dilute HNO_3). Cap the vials with their original caps and leave to stand a few hours. The fluorides should dissolve totally to give a clear (or perhaps faintly green) solution.
9. Weigh and record the vial+solution weights.

10. Invert the capped vials a few times to homogenise the solutions, decant them into labelled centrifuge tubes and send them off for ICP analysis.

Clean the Teflon ware using the procedure outlined in General Lab Practice.

Parent Solution Dry Down and Chloride Conversion

Successive evaporation and re-dissolution eliminates fluoride (as HF) almost entirely. Fe, Ti, Al, Be, alkalis etc. should be left as chloride salts ready for anion exchange clean-up. The final solution will generally be coloured a deep yellow-green by $FeCl_3$. By the end of this procedure, however, some samples may have thrown a fine, powdery, white precipitate that will not re-dissolve. This is TiO_2. No Al or Be is co-precipitated with the Ti, which should be removed by centrifuging before moving on to the anion exchange columns.

Procedure

1. Carefully transfer the parent solution to a clean and labelled Teflon beaker (250 or 500 ml).
2. Rinse the bottle with a few ml of MilliQ and add the rinsate to the beaker. Take care not to let any sample solution splash back onto the MQ wash bottle.
3. Using separate disposable transfer pipettes add 2-3 ml of 6M HCl and 1ml of 8M HNO_3 to each beaker.
4. Place the beakers on the hotplate and dry at setting 4 (~90°C-140°C) overnight; during the day temperature can be increased up to set 5 (130°C –180°C). For <100 ml, the beakers will dry down in 12 - 15 hours. Larger solution volumes may take a bit longer. When drying large volumes droplets will condense on the rim of beakers, do not worry they will dry off. When dry, there will be a thin covering of white to gray-green fluoride salts on the floor of the beaker. There may also be some residual tiny droplets on the beaker walls - don't worry about these.

To convert the residue to chloride form...

5. Take the beakers off the hotplate and cool them. Using a disposable pipette, add ~2 ml of 6N HCl (the amount is not critical; samples with a very large fluoride cake may require a little more). The cake should mostly re-dissolve instantaneously, and in most cases will go back into solution entirely after warming on the hotplate.
6. Return the beakers to the hotplate and dry again at setting 4 (~90°C-140°C).
7. Cool and repeat the 6N HCl addition.
8. Dry again, cool and re-dissolve a third time, then take down as close to dryness as possible. Try to avoid complete drying at the end of this step, to make it easy to get the sample back into solution for anion exchange. Don't worry if drying is unavoidable, however.
9. Add 2 ml of 6N HCl to each sample container. The precise volume is not critical and can be measured from the marks on a disposable pipette. Swirl the liquid to pick up and dissolve the entire sample from the floor of the container. Leave standing overnight. Do not warm to promote dissolution - evaporation will lower the acid

strength. This step can be carried out as step 7 in the Anion Exchange procedure but carrying it now will facilitate total sample's dissolution.

Ion Exchange

Anion exchange columns are used to separate remaining impurities such as Fe and Ti from the sample. In strong HCl, Fe(III) forms a range of anionic Cl^- complexes ($FeCl_4^-$, $FeCl_5^{2-}$ and $FeCl_6^{3-}$), which bind tightly to the anion exchange resin. These can be seen as a brown stain in the top few mm of the resin. Al and Be do not form strong Cl^- complexes and wash through the column as HCl is added. Titanium is a bit more problematic; Ti(IV) forms $TiCl_6^{2-}$, which binds, but some Ti always seems to remain cationic, form neutral species or revert to Ti(III), which doesn't form strong Cl^- complexes. Ti is seldom 100% stripped from the Al + Be fraction. Al and Be are split and Ti is further removed using cation exchange columns.

Procedure for Anion Exchange CHROMATOGRAPHY

AX chromatography may take up to 4 hours. (6ml takes ~30' to be eluted)

1. Load a column stand with ion exchange columns. Place a plastic container underneath.
2. Squirt some alcohol (ethanol, isopropanol, whatever is on hand) into each to wet the frit (to eliminate trapped air).
3. Using AG-1 X8 200-400# anion resin from stock soaking in 1.2N HCl, pipette a very **loose slurry** into each column (use a disposable pipette). The aim is to block the column and back up a head of acid so that the resin bed can be built up from suspension. This prevents trapping of air bubbles.
4. Now continue slurrying resin into the columns to build 2 ml resin beds. If too much resin is added, a long pasteur pipette can be used to adjust the volume. If too thick a slurry is added and bubbles get trapped in the bed, the column must be emptied and re-packed. Bubbles will channel flow through the column and ruin the separation. Once the resin has compacted to the correct height, allow the supernatant to drain through.
5. Wash the resin with 10ml HCl (1.2M ("10%") HCl is convenient, though more dilute HCl does a better job. Allow the wash solution to drain through the resin bed.
6. Condition the resin with 10ml 6N HCl. Add the first ml by running drops down the column walls - try to keep the top surface of the resin bed flat to ensure uniform flow through the column when the sample is added. The resin will darken and shrink as it adjusts to the higher acid strength (it may not be noticeable).
7. While the conditioning solution is draining, add 2 ml of 6N HCl to each sample container. The precise volume is not critical and can be measured from the marks on a disposable pipette. Swirl the liquid to pick up and dissolve the entire sample from the floor of the container. Do not warm to promote dissolution - evaporation will lower the acid strength.
8. Check the sample for any signs of smoky white insoluble material (this will be TiO_2). If any is present, solutions will have to be centrifuged before running them through the columns. To do this, transfer solutions to labelled disposable 12 ml centrifuge tubes

using a clean disposable pipette for each sample. Add a further ml of 6N HCl to the sample containers as a rinse. Pick the rinse solution up and add them to their appropriate centrifuge tubes.

9. **CENTRIFUGE**: *Make sure that the loads in the centrifuge are balanced. Use a massed dummy tube if there is a spare slot in the centrifuge.*
10. Spin the tubes at maximum speed (notionally 3200 RPM) for 10 minutes. The pipettes used for each sample should be reserved (in the original sample containers) for loading.
11. Take a batch of 20 ml Teflon vials and label them with sample ID.
12. Once the 6M HCl conditioning solutions have drained, carefully remove the plastic container from beneath the columns and replace them with 20 ml Teflon vials. The HCl in the container should be disposed in the acid waste container.
13. Using separate disposable pipette for each sample (those centrifuged will already have one), load the sample solutions onto the columns. Drip the solution down the column wall, reaching as far as possible into the column with the pipette. Do NOT pour the sample into the column. Try to transfer the sample quantitatively. Try not to disrupt the top surface of the resin. Return each pipette to its sample container.
14. Add 1 ml of 6M HCl to the sample containers and swirl to pick up any remaining droplets of the original sample solution. This step is not necessary for samples that were centrifuged or transferred to centrifuge tubes and have already been washed out of their containers.
15. Allow the loading solution to drain fully into the resin. Now add the 1 ml wash solutions where appropriate. Allow to drain into the resin.
16. Elute Al + Be from the columns by adding 6ml 6M HCl. The first ml should be added carefully from a disposable pipette so as not to disrupt the top of the resin bed.
17. Once Al + Be have been eluted, remove the vials and replace them with labelled 15ml bottles.
18. Add 1 drop of 2% H_2O_2 to each vial. Change of colour to yellow-orange indicates the presence of Ti in the fraction. Note changes to monitor fractions during following sample prep steps.
19. Add 1 ml of 0.5M H_2SO_4 (500 µmol) to each vial and dry on the hotplate overnight. Dry at setting 3 ¼ (70°C-90°C) to avoid boiling the sample. The following sample prep steps are indicated in the next section (***To convert the residue to sulphate form***).
20. Wash Fe + Ti off the resin with 10ml MQ water. (Fe reverts to the cationic ± $FeCl_3^0$ form - HCl will drip yellow-green after a few ml). Rinse out and discard the sample and dispensing pipettes. Rinse out and wash the sample transfer containers.
21. Rinse out resin and clean the columns as described under Laboratory Cleanliness.

To convert the residue to sulphate form...

Once the samples have dried down they may turn an alarming dark-brown to black colour. This is due to chary reaction products formed from organics which bled from the anion resin. Don't worry, it will disappear gradually over the next few steps.

22. Cool the vials. Add 5-6 drops of ~2% H_2O_2. Add 2ml MilliQ containing a trace of 0.5M H_2SO_4 (Solution~0.0368 M H_2SO_4 prepared by adding 2ml 1:1 H_2SO_4 to 500 ml MQ water) (~74 µmol). The cakes will begin to dissolve, taking on an amber/gold color ($TiO[H_2O_2]^{2+}$) if Ti is present. Reheat the vials. The black charry material will

disperse and disappear (do not worry if it does not happen straight away; the heat applied will help the dispersion).

23. Dry the samples down again (max at set 4 (90°C -150°C) if you are in the lab; set 3 if left overnight). The H_2O_2 oxidises the organics. It also indicates the presence of Ti in the sample by turning the solution yellow-orange. The darker the colour, the more Ti is present.
24. Cool the vials and repeat the H_2O_2/MilliQ water addition, and dry the samples a second time. At the end of this procedure, the samples should end up either as compact white cakes; small, syrupy droplets of involatile H2SO4 or orange/yellow syrupy cakes. If they remain charry or discolored, repeat the peroxide/water addition and dry them down as many times as necessary
25. Take the sample up (as a cake or 1-2 drops) in 2ml H_2O containing a trace of 0.5M H_2SO_4. Add 1 drop of ~2%H_2O_2. Leave overnight.
If sample does not contain Ti (e.g. 2nd CX, take sample up in 2ml 1.2 M HCl. Transfer to centrifuge tube. Rinse beaker with 1ml 1.2 M HCl and add rinsate to appropriate centrifuge tube).
26. If samples do not dissolve completely after leaving overnight warm them a little. Don't risk evaporating too much water – keeping the acid strength low for column loading gives a sharper elution and cleaner Ti-Be cut. The samples are now in ~0.398 M H_2SO_4 *(500+ (4*74))µmol/2ml) as addition/dry down is carried out a total of 3 times on average.*
27. Transfer sample to a labelled centrifuge tube. Add a further ml of 0.5M H_2SO_4 (500 µmol) (final concentration ~ 0.432M H_2SO_4) with a trace of H_2O_2 to the sample containers and rinse. Swirl to pick up any remaining droplets of the original sample solution. Pick the rinse solution up and add to their appropriate centrifuge tubes. If necessary (dissolution is not complete) centrifuge sample and keep centrifuge tube with residue material until results are obtained. If sample is fully dissolved centrifugation is not necessary. The samples can be stored indefinitely in centrifuge tubes.
28. The samples are now ready for cation exchange to remove Ti and to split Be and Al into separate fractions.

Procedure for cation exchange chromatogrqaphy

CX chromatography may take up to 7 hours. (10ml takes ~30' to be eluted)

1. Load a column stand with ion exchange columns. Place a plastic container underneath.
2. Squirt some alcohol (ethanol, isopropanol, whatever is on hand) into each to wet the frit.
3. Using AG 50W - X8 200-400# cation resin from stock soaking in dilute HCl (1.2 M HCl) , pipette a very loose slurry into each column (use a disposable pipette). The aim is to block the column and back up a head of acid so that the resin bed can be built up from suspension. This prevents trapping of air bubbles.
4. Now continue slurrying resin into the columns to build 2 ml resin beds. If too much resin is added, a long pasteur pipette can be used to adjust the volume. If too thick a slurry is added and bubbles get trapped in the bed, the column must be emptied and re-packed. Bubbles will channel flow through the column and ruin the separation. Once the resin has compacted to the correct height, allow the supernatant to drain through.
5. Strip the columns with 10ml (up to top of column holder) 4M HCl followed by 10ml 1.2M HCl.
6. Condition the columns with 10ml 0.2M H_2SO_4 (with a trace of H_2O_2)

7. Once the 0.2M H_2SO_4 conditioning solutions have drained, carefully remove the plastic beaker from beneath the columns and replace them with labelled 15 ml plastic bottles.
8. Using separate disposable pipettes for each, load the sample solutions onto the columns. Drip the solution down the column wall, reaching as far as possible into the column with the pipette. Do NOT pour the sample into the column. Try to transfer the sample quantitatively. Try not to disrupt the top surface of the resin. Return each pipette to its sample container.
9. Allow the loading solution to drain fully into the resin. If present Ti will have formed an orange band at the top of the column.
10. Add a total of 8ml 0.5M H_2SO_4 with a trace of H_2O_2 to the columns but **PIPETTING the first ml** to avoid disturbing the resin. Allow to drain through before adding the remaining 7 ml (DO NOT TRANSFER DIRECTLY, PIPETTE THE FIRSTS mls) and watch the band of Ti move down the column.
11. If not all Ti has been eluted (elutant/tip are yellow and/or orange band in the resin), add 1 - 2 ml 0.5M H_2SO_4 with a trace of H_2O_2. Do not add more than 2ml as Be will start to be eluted then. If not all Ti is eluted after the further 2mls added make a note of the sample and Ti will be separated from fraction by precipitating it at pH 4 (***see Precipitation as Hydroxides***)
12. Replace the bottles with labelled 20ml Teflon vials.
13. Elute Be from the columns by adding 10ml 1.2 N HCl. The first few ml should be added carefully from a disposable pipette so as not to disrupt the top of the resin bed. (Yellow elutant indicates the presence of Ti)
14. Once the columns have drained replace the vials with labelled 15ml centrifuge tubes.
15. Add 5 drops of 8M HNO_3 to the Teflon vials dry them down overnight at setting 2 ¾ (~60C) to avoid total dryness if possible.
16. Elute Al from the columns by adding 6ml of 4M HCl. The first few ml should be added carefully from a disposable pipette so as not to disrupt the top of the resin bed. Once the columns have drained cap the tubes and store them until hydroxide precipitation.
17. Clean the columns as described under Laboratory Cleanliness.

If sample does not contain Ti proceed with step 1 to 5 as indicated. Load sample and 1 ml wash to column then follow up from step 12 onwards.

Precipitation as Hydroxides

Procedure

Be fraction

1. Once the Be solutions have dried down (near dryness as possible), cool the vials. There should only be a small white dot or small drop in the bottom of the vials.
2. Add 2ml 1%HNO_3 to the vials. The Be should dissolve readily. If it doesn't you can heat the vials to assist dissolution.
3. Transfer the solutions to labelled 15ml centrifuge tubes.
4. Add another 1ml 1% HNO_3 to the vials, swirl it around and transfer the rinse solution to the appropriate tube.

5. If Ti is present in sample use 10%-20% NH_4OH solutions to bring pH up to 4. Ti will precipitate as hydroxide whilst Be will remain in solution. Centrifuge the solutions at 3500rpm for 10 minutes. Decant and collect supernatant (Be fraction) in ~15 ml centrifuge tubes. Precipitate is Ti hydroxide.
6. Using 25%-50% NH_4OH solutions, bring Be solutions in the 15 ml centrifuge tubes to pH 8 (beyond pH 10 Be will re-dissolve) to precipitate Be as a hydroxide. Addition of ammonium hydroxide may have to be drop by drop with pH checks in-between. Leave the tubes standing for a few hours. (To speed up precipitation you can place the tubes into a warm water bath).
7. Centrifuge the solutions at 3500rpm for 10 minutes.
8. Decant and discard the supernatant into the acid waste tank.
9. Rinse the samples with 5 ml MilliQ water and 1 drop 25% NH_4OH added to the centrifuge tubes.
10. Disperse the samples by vortexing (until precipitate is re-dissolved)
11. Centrifuge again at 3500rpm for 10 minutes.
12. Decant and discard the supernatant into the acid waste tank.
13. Repeat the MilliQ + NH_4OH rinse three times.

Al fraction

1. Using conc. - 50% NH_4OH solutions, bring Al fraction (in 6mls 4MHCl) in the 15 ml centrifuge tubes to **pH 8** (beyond pH 10 Al will re-dissolve) to precipitate Al hydroxide. **Always start with conc. NH_4OH** solution. Addition of ammonium hydroxide may have to be drop by drop with pH checks in-between. Leave the tubes standing for a few hours. (To speed up precipitation you can place the tubes into a warm water bath). Reaction is exothermic. (Al precipitation is initially not as easy to see as Be precipitation)
2. Centrifuge the solutions at 3500rpm for 10 minutes.
3. Decant and discard the supernatant into the acid waste tank.
4. Rinse the samples with 5 ml MilliQ water and 1 drop 25% NH_4OH added to the centrifuge tubes.
5. Disperse the samples by vortexing (until precipitate is re-dissolved)
6. Centrifuge again at 3500rpm for 10 minutes.
7. Decant and discard the supernatant into the acid waste tank
8. Repeat the MilliQ + NH_4OH rinse three times.

DO NOT store Al and Be as hydroxides in alkaline solutions (salts are formed under this condition). It is OK to store them as fractions collected after CX chromatography (acid solutions) or as dry hydroxides.

Drying and Oxidation

Procedure

1. Carefully open the 15 ml centrifuge tubes containing the Be and Al hydroxides and lie them on a kimwipe in the drying oven. It helps to put a folded kimwipe under the open ends to keep them slightly elevated. Keep track of which lid belongs to which tube. Cover the tubes with a kimwipe and dry overnight at 70°C.

2. When dry, cap the 15 ml centrifuge tubes with their respective lids and let them cool. (Tap them slightly to free the oxide).
3. Weigh a cleaned quartz crucible and lid to 4 decimal places (*for instructions on cleaning quartz crucibles see Laboratory Cleanliness*). Place the crucible into the perspex holder. On a piece of paper write down the relative positions of the quartz crucibles and the Sample ID of the sample which will be transferred into them.
4. **For Be hydroxides**: In the Be box, wearing a new pair of gloves, and a face mask pour the small pellet of dried Be hydroxide over a clean weighing paper and transfer it to the quartz crucible. Use the help of a spatula if the pellet does not come off the walls of the centrifuge tube easily. If you experience problems with static electricity; use the anti-static device or wrap tubes with foil paper. Pour the pellet over a clean weighing paper and transfer it to the quartz crucible. Cover the quartz crucible with its respective quartz lid. Place the crucibles in their position in the Perspex holder. Avoid sample cross contamination.
   For Al Hydroxides: Same as for Be hydroxide but the transfer can be done on the open lab bench without the need of the face mask.
5. Transfer perplex holder to the furnace. Place crucibles (covered with lids) inside the furnace making sure that the relative positions of the crucibles is maintained.
6. Bake the crucibles at 800 °C for 2 hours. (*The furnace is programmed for this*)
7. Let the furnace and crucibles cool down (15 hours).
8. Remove the crucibles from the furnace, weigh them and subtract the tare weight to get the weight of the oxides. Transfer them to the perplex holder keeping their relative position.
9. Al oxides will be pressed in the AMS lab. Carefully transfer the perplex holder (with oxides) to a plastic box and take to the AMS lab. Be oxides will be pressed in the CIF-CfG lab (Room 8 at SUERC)

7.2 Chemistry Data

	PROCESS: *Quartz Aliquot Digestion and Al Assay*			
SAMPLE	sample(g)	soln (g)	[Al] soln (ppm)	[Al] qtz (ppm)
GR0601	0.3556	8.1231	1.07	24.4
GR0606	0.3188	8.1209	1.76	44.8
GR0603	0.2098	8.1491	1.71	66.4
GR0604	0.3671	8.1131	1.16	25.6
GR0605	0.4818	8.1168	12.59	212.09
GR0606	0.4426	8.1531	1.23	22.7
GR0607	0.2443	8.0666	2.28	75.3
GR0608	0.4356	8.1093	1.38	25.7
GR0609	0.3238	8.1244	1.83	45.9
	PROCESS: Quartz Sample Digestion			
SAMPLE	Bottle tare (g)	With sample (g)	Sample (g)	vol HF req (ml)
GR0601	112.083	132.986	20.903	105
GR0606	112.847	133.081	20.234	101
GR0603	107.281	128.606	21.325	107
GR0604	107.694	128.196	20.502	103
GR0605	109.343	128.442	19.099	95
GR0606	107.242	127.137	19.895	99
GR0607	106.845	120.133	13.288	67
GR0608	107.281	128.026	20.745	104
GR0609	112.35	133.201	20.851	104
	PROCESS: Be Spike			
SAMPLE	mass of Be bottle (g)	mass removed (g)	final mass of bottle (g)	carrier id
GR0601	89.103	0.8296	88.1834	TCW III
GR0606	88.1834	0.8282	87.3552	TCW III
GR0603	87.3552	0.8291	86.5261	TCW III
GR0604	86.5261	0.8286	85.6975	TCW III
GR0605	135.6425	0.8287	134.8138	TCW IV
GR0606	85.6975	0.8289	84.8696	TCW III
GR0607	132.3167	0.8291	131.4876	TCW IV
GR0608	84.8696	0.8283	84.0403	TCW III
GR0609	84.0403	0.8278	83.2125	TCW III
	PROCESS: Splitting for Al determination			
SAMPLE	bottle and soln (g)	mass parent soln (g)	~Al ppm in parent soln	ICP aliquot (ml)
GR0601	268.909	156.826	8.6	~8.1
GR0606	269.637	156.79	11.1	~6.3
GR0603	256.589	149.308	9.5	~7.4
GR0604	266.251	158.557	8.6	~8.1
GR0605	261.745	152.402	26.6	~2.6
GR0606	269.002	161.76	8	~8.8
GR0607	231.902	125.057	8	~8.8
GR0608	259.887	152.606	9	~7.8
GR0609	263.904	151.554	11.8	~5.9
	PROCESS: Dry down and dilution			
SAMPLE	split mass (g)	ICP soln (g)		
GR0601	9.7737	10.1526		
GR0606	7.6661	10.1443		

GR0603	9.4861	10.142		
GR0604	10.1028	10.1699		
GR0605	3.2816	9.2238		
GR0606	10.7385	10.1919		
GR0607	10.4631	10.2151		
GR0608	9.8548	10.1848		
GR0609	7.2283	10.1023		
	Yield			
SAMPLE	BeO (g)			
GR0601	0.0005			
GR0606	0.0006			
GR0603	0.0006			
GR0604	0.0004			
GR0605	0.0029			
GR0606	0.0006			
GR0607	0.0004			
GR0608	0.0004			
GR0609	0.0005			

7.3 AMS Data

Cathode No	Sample ID	$^{10}Be/^{9}Be$	σ ($^{10}Be/^{9}Be$)	$^{10}Be/^{9}Be$ ($x10^{-15}$)	σ ($^{10}Be/^{9}Be$) ($x10^{-15}$)
b1470	GGR0601	1.24E-13	4.86E-15	123.88	4.86
b1471	GGR0602	9.66E-14	3.55E-15	96.61	3.55
b1472	GGR0603	9.51E-14	3.38E-15	95.14	3.38
b1473	GGR0604	9.51E-14	3.33E-15	95.12	3.33
b1474	GGR0606	8.07E-14	2.99E-15	80.70	2.99
b1477	GGR0608	7.48E-14	4.11E-15	74.80	4.11
b1478	GGR0609	7.73E-14	4.02E-15	77.32	4.02
b1479	GGR0605	6.31E-14	5.58E-15	63.10	5.58
b1480	GGR0607	5.65E-14	6.85E-15	56.47	6.85